HEALTH AND MEDICINE

Activation of PDGFRA signaling contributes to filamin C–related arrhythmogenic cardiomyopathy

Suet Nee Chen[1]*†, Chi Keung Lam[2,3,4]†, Ying-Wooi Wan[5], Shanshan Gao[1], Olfat A. Malak[2,3], Shane Rui Zhao[2,3], Raffaella Lombardi[1,6], Amrut V. Ambardekar[1], Michael R. Bristow[1], Joseph Cleveland[1], Marta Gigli[7], Gianfranco Sinagra[7], Sharon Graw[1], Matthew R.G. Taylor[1], Joseph C. Wu[2,3,8]*, Luisa Mestroni[1]*

Copyright © 2022 The Authors, some rights reserved; exclusive licensee American Association for the Advancement of Science. No claim to original U.S. Government Works. Distributed under a Creative Commons Attribution NonCommercial License 4.0 (CC BY-NC).

***FLNC* truncating mutations (*FLNCtv*) are prevalent causes of inherited dilated cardiomyopathy (DCM), with a high risk of developing arrhythmogenic cardiomyopathy. We investigated the molecular mechanisms of mutant FLNC in the pathogenesis of arrhythmogenic DCM (a-DCM) using patient-specific induced pluripotent stem cell–derived cardiomyocytes (iPSC-CMs). We demonstrated that iPSC-CMs from two patients with different *FLNCtv* mutations displayed arrhythmias and impaired contraction. FLNC ablation induced a similar phenotype, suggesting that *FLNCtv* are loss-of-function mutations. Coimmunoprecipitation and proteomic analysis identified β-catenin (CTNNB1) as a downstream target. FLNC deficiency induced nuclear translocation of CTNNB1 and subsequently activated the platelet-derived growth factor receptor alpha (PDGFRA) pathway, which were also observed in human hearts with a-DCM and *FLNCtv*. Treatment with the PDGFRA inhibitor, crenolanib, improved contractile function of patient iPSC-CMs. Collectively, our findings suggest that PDGFRA signaling is implicated in the pathogenesis, and inhibition of this pathway is a potential therapeutic strategy in FLNC-related cardiomyopathies.**

INTRODUCTION

Dilated cardiomyopathy (DCM) is the most common inherited cardiomyopathy and is a leading cause of sudden cardiac death and heart failure, particularly in young adults. (*1*–*4*). The prevalence of DCM is approximately 1:250 (*5*). In the United States, the annual cost of managing DCM has been estimated to be approximately $4 billion to $10 billion. Ventricular arrhythmia is a major cause of morbidity and mortality in patients with DCM (*4*). Notably, carriers of filamin C (*FLNC*) truncating mutations are at high risk of developing dilated and arrhythmogenic cardiomyopathies (*6*, *7*). We previously identified truncation mutations in *FLNC* as a cause of arrhythmogenic DCM (a-DCM), which implicates *FLNC* as a previously unidentified a-DCM causal gene (*6*). Thus, it becomes important to understand the roles of *FLNCtv* mutations in the pathogenesis of a-DCM to develop effective targeted treatment.

FLNC is an isoform of the filamin family, predominantly expressed in skeletal and cardiac muscle (*8*, *9*). Mutations in *FLNC* have been associated with myofibrillar skeletal myopathies, hypertrophic cardiomyopathy, restrictive cardiomyopathy, DCM, and arrhythmogenic cardiomyopathy (ACM) (*10*–*12*). FLNC is an actin binding protein and is known to localize to the Z-discs and the intercalated discs (ID). FLNC modulates cell stiffness by regulating cross-linking of actin filaments and anchorage of the actin-cytoskeleton to transmembrane proteins at cell-cell adhesion sites (*8*, *9*). Because of its interactions with transmembrane and Z-disc proteins, mutations in *FLNC* would be expected to dysregulate intracellular signaling. However, signaling functions of FLNC in cardiac myocytes are not currently known. Moreover, the precise molecular mechanisms that cause arrhythmias due to *FLNCtv* mutations are largely unknown.

Numerous studies have shown that platelet-derived growth factor (PDGF) signaling is an important regulator of cardiogenesis (*13*–*15*). Previously, our cell fate lineage studies have shown that PDGF receptor alpha (PDGFRA)–positive progenitor cells contribute to a subpopulation of cardiac myocytes (*16*). PDGFRA is a transmembrane tyrosine kinase receptor activated by PDGFA and PDGFC (*17*, *18*). During cardiac development, PDGFRA is implicated in a spectrum of physiologic and pathologic processes, including cell growth and survival (*19*, *20*), stem cell differentiation (*16*, *21*), and migration (*13*, *22*). Following development, both alpha and beta cardiac PDGFRs become silent. However, abnormal PDGFRB activation has been implicated in the pathogenesis of cardiomyopathy induced by lamin-A/C (*LMNA*) mutations (*23*). In tumorigenesis studies, PDGFR activation has been shown to promote the activation of intracellular signaling pathways such as Ras/MAPK (mitogen-activated protein kinase) and phosphatidylinositol 3-kinase (PI3K)/Akt (*24*, *25*). However, the molecular mechanisms governing PDGFR activation and downstream signaling in cardiac myocytes remain largely unknown.

In the present study, we aimed to identify the downstream molecular mechanisms involved in the pathogenesis of *FLNCtv* cardiomyopathies. Our data indicated significant up-regulation of PDGFRA signaling in FLNC-mutant induced pluripotent stem cell–derived cardiomyocytes (iPSC-CMs) compared to isogenic iPSC-CMs, leading us to investigate the role of PDGF receptor signaling activation on arrhythmogenesis in FLNC mutant cardiac myocytes and ultimately to examine the potential of PDGFR inhibition in rescuing FLNC-related cardiomyopathy.

[1]University of Colorado Cardiovascular Institute, University of Colorado Anschutz Medical Aurora, CO, USA. [2]Stanford Cardiovascular Institute, Stanford, CA, USA. [3]Department of Medicine, Division of Cardiovascular Medicine, Stanford University School of Medicine, Stanford, CA, USA. [4]Department of Biological Sciences, University of Delaware, Newark, DE, USA. [5]Department of Molecular and Human Genetics, Baylor College of Medicine, Houston, TX, USA. [6]Department of Advanced Biomedical Sciences University of Naples "Federico II", Naples, Italy. [7]Cardiovascular Department, Azienda Sanitaria-Universitaria Giuliano Isontina (ASUGI), Trieste, Italy. [8]Department of Radiology, Stanford University School of Medicine, Stanford, CA, USA.
*Corresponding author. Email: suet.chen@cuanschutz.edu (S.N.C.); joewu@stanford.edu (J.C.W.); luisa.mestroni@cuanschutz.edu (L.M.)
†These authors contributed equally to this work.

Downloaded from https://www.science.org at Universita degli Studi di Trieste on March 30, 2022

RESULTS

Modeling FLNC-related DCM using patient-specific iPSC-CMs

We recruited two family cohorts with patients carrying truncating mutations in *FLNC*: G1891Vfs61X and E2189X (*7*, *26*). Affected individuals with the G1891Vfs61X mutation were diagnosed with a-DCM with clinical presentation of polymorphic sustained ventricular tachycardia, paroxysmal atrial fibrillation, and depressed left ventricular systolic function (*7*), while affected family members with E2189X mutation were diagnosed with arrhythmogenic right ventricular cardiomyopathy (ARVC) with clinical presentation of nonsustained ventricular tachycardia with left bundle branch block morphology and frequent ventricular extrasystoles (*26*). Clinically affected individuals from both families with the truncating mutations presented with cardiac restricted phenotypes without skeletal muscle anomalies. Overall, these affected individuals from both families exhibited cardiac arrhythmias with DCM.

Next, we generated iPSC lines from patients who carried the respective truncating mutations using nonintegrating reprogramming methods (*27*). We differentiated the iPSCs into iPSC-CMs using a chemically defined protocol for subsequent electrophysiological properties and molecular mechanism delineation studies (*28*). We found that iPSC-CMs from both patients with *FLNCtv* showed weaker contraction and slower relaxation, compared to healthy controls (Fig. 1, A and B, and fig. S1). The observed phenotype is most likely attributed to dysregulation of genes involved in contractility (fig. S2). Both lines of patient-specific iPSC-CMs also exhibited spontaneous arrhythmia (Fig. 1C). The arrhythmic phenotype was also indicated by larger variations in beating rate as compared to control iPSC-CMs (Fig. 1D). To further validate the arrhythmic phenotype, we examined the action potential (AP) morphology of both healthy and patient iPSC-CMs. Consistent with the contraction data, 40% of $FLNC^{G1891Vfs61X}$ and 36% of $FLNC^{E2189X}$ iPSC-CMs exhibited abnormal AP morphology as compared with the two lines of control iPSC-CMs (Fig. 1, E and F). Together, these data show that FLNC patient iPSC-CMs recapitulate the arrhythmia phenotype associated with FLNC-related DCM in vitro.

$FLNC^{G1891Vfs61X}$ and $FLNC^{E2189X}$ are loss-of-function mutations that lead to haploinsufficiency in FLNC-related cardiomyopathy

We next examined the expression levels of FLNC in the patient-specific iPSC-CMs and found that both $FLNC^{G1891Vfs61X}$ and $FLNC^{E2189X}$ mutants expressed significantly lower FLNC protein and mRNA levels compared to control iPSC-CMs as detected by immunoblots and quantitative polymerase chain reaction (qPCR) (Fig. 2, A to C). Despite the reduced expression levels, we were able to detect FLNC and its colocalization with α-actinin at Z-disc by immunofluorescence staining and colocalization analysis, in both FLNC-mutant iPSC-CM lines (Fig. 2D).

To investigate whether $FLNC^{G1891Vfs61X}$ and $FLNC^{E2189X}$ were loss-of-function mutations, we generated FLNC-deficient iPSC lines and isogenic control lines for differentially expressed gene (DEG) profiles in comparison with DEG profiles from patients' iPSC-CMs. As shown in Fig. 2 (E to H) and fig. S3, we successfully generated FLNC homozygous ($FLNC^{KO-/-}$) and heterozygous ($FLNC^{KO+/-}$) knockout (KO) iPSC-CMs. The FLNC expression levels were significantly reduced in $FLNC^{KO-/-}$ and $FLNC^{KO+/-}$ iPSC-CMs in an allele-dependent fashion at both mRNA and protein levels as detected by qPCR and immunoblots. Moreover, FLNC was not detected at the Z-disc by immunofluorescence staining and colocalization analysis in the FLNC KO lines (Fig. 2H). $FLNC^{KO-/-}$ iPSC-CMs showed α-actinin disorganization indicating disturbed sarcomere organization (Fig. 2H). Notably, RNA sequencing (RNA-seq) bioinformatics analysis demonstrated a positive correlation between the DEGs in *FLNC* truncating mutations and those in *FLNC* KO iPSC-CMs, supporting loss of function as the main mechanism through which *FLNC* mutations cause the phenotypic manifestations (Fig. 2I). In addition, iPSC-CMs carrying *FLNC* mutations had significantly decreased levels of ID proteins; the same finding was observed in *FLNC* KO iPSC-CMs (Fig. 2J). Last, $FLNC^{KO-/-}$ cells exhibit a similar arrhythmic phenotype to the patient iPSC-CMs (Fig. 1, E and F). Together, the data support the notion that $FLNC^{G1891Vfs61X}$ and $FLNC^{E2189X}$ truncating mutations lead to haploinsufficiency. In addition, bioinformatics analysis suggested that loss of FLNC affected the integrity of Z-discs and IDs in cardiomyocytes as evidenced by down-regulation of Gene Ontology (GO) biological function pathways involved in cardiac contraction and sarcomere organization (fig. S4).

The loss of FLNC causes nuclear localization of β-catenin and activation of the β-catenin signaling pathway

To discover the partners of FLNC, we performed coimmunoprecipitation followed by proteomic analysis and identified β-catenin through proteomic analysis. The proteomic data were confirmed by immunoblots (Fig. 3A). We did not detect β-catenin in the pull-down lysates from $FLNC^{KO-/-}$ iPSC-CMs and there was also a reduced amount of β-catenin in the pull-down lysate from FLNC-mutant iPSC-CMs (Fig. 3A and fig. S5A). Furthermore, we detected significant amounts of β-catenin in the nuclei of FLNC-mutants and $FLNC^{KO-/-}$ iPSC-CMs in contrast to control iPSC-CMs in which β-catenin was mainly detected in the cytoplasm (Fig. 3, B and C). In addition, expression profiles on RNA-seq data from $FLNC^{KO-/-}$ and FLNC-mutant iPSC-CMs showed activation of β-catenin signaling [The Database for Annotation, Visualization and Integrated Discovery (DAVID); GO000813_92G] (Fig. 3D). In addition, gene set enrichment using the Molecular Signature Database HALLMARK_WNT_BETA_CATENIN_SIGNALING showed a trend similar to the β-catenin signaling gene set cataloged in DAVID (fig. S5, B to D). Together, our data demonstrate that β-catenin is possibly a novel binding partner as well as a downstream effector of FLNC and that the loss of FLNC in iPSC-CMs caused the migration of β-catenin from the cytosol to the nucleus leading to β-catenin signaling activation.

To examine the potential of targeting β-catenin signaling in patients with *FLNC*, we next performed rescue experiments by pharmacologically inhibiting β-catenin in mutant FLNC iPSC-CMs to determine whether treatment could improve contractility of cardiac myocytes. We treated *FLNC* patients' iPSC-CMs with two β-catenin inhibitors, JW74 and JW67, at increasing concentration (100 nM, 1 μM, and 10 μM) and measured contractility on treatment days 0, 3, and 7. β-Catenin inhibition failed to improve contractility of the patients' iPSC-CMs (figs. S6 and S7), suggesting that β-catenin signaling may be too upstream to the disease-causing signaling cascades, or that blockade of β-catenin may also affect other important pathways in cardiomyocytes. We then tested the hypothesis that a more downstream effector may be a better therapeutic target for patients with FLNC.

Downloaded from https://www.science.org at Universita degli Studi di Trieste on March 30, 2022

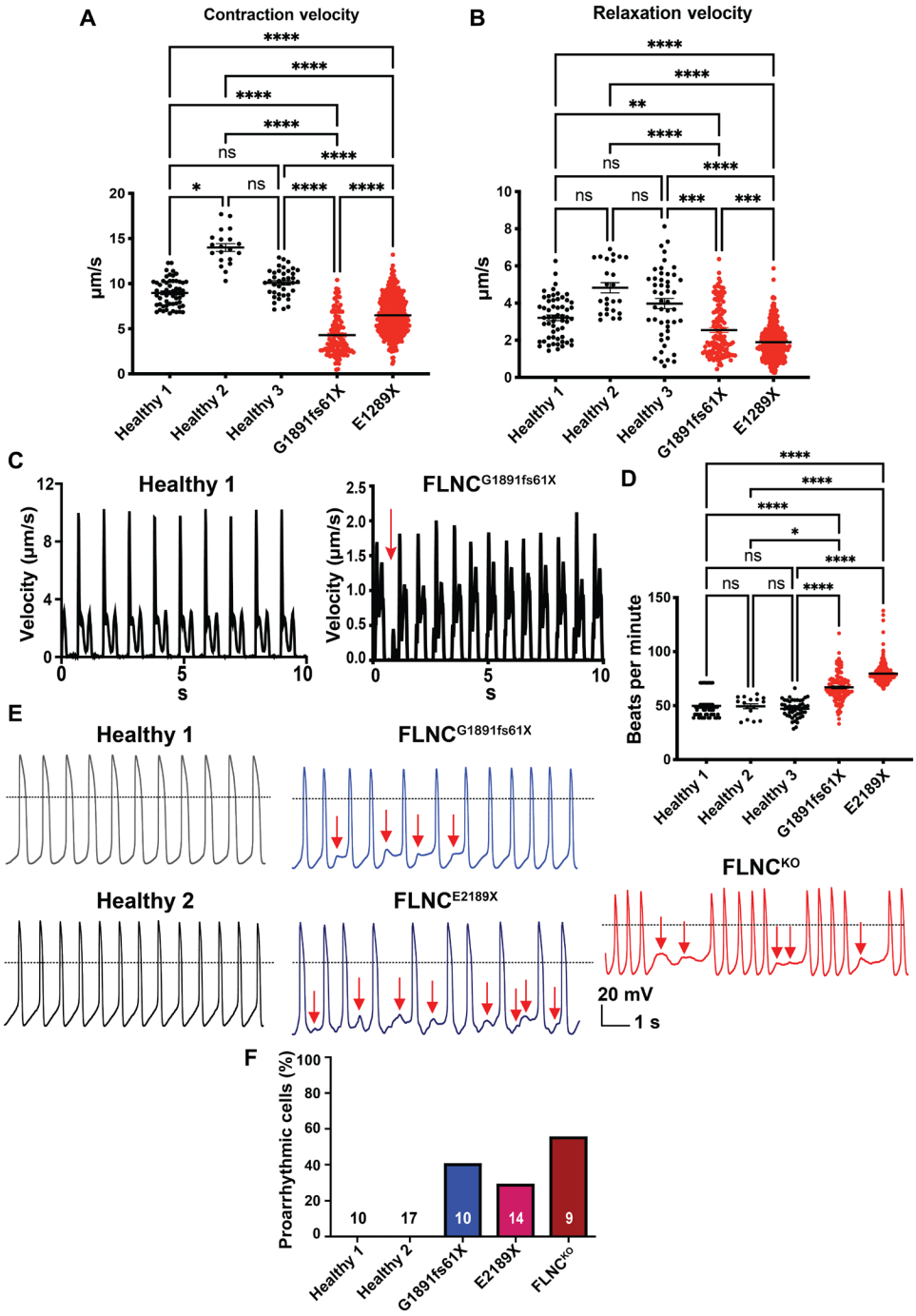

Fig. 1. FLNC^{G1891Vfs61X} and FLNC^{E2189X} iPSC-CMs exhibited impaired contractility and arrhythmia. (**A**) Contraction and (**B**) relaxation velocities of both patient-derived iPSC-CMs were lower than those of healthy controls ($n = 20$ to 400 replicates from two different batches). (**C**) Representative contraction traces of healthy control iPSC-CMs and FLNC^{G1891Vfs61X} iPSC-CMs suggest spontaneous arrhythmia in the patient cells (red arrow). (**D**) Beating rate variations were higher in both patient-derived iPSC-CM lines ($n = 20$ to 400 replicates from two different batches). (**E**) Representative spontaneous action potential recordings from healthy and arrhythmic iPSC-CMs. Healthy iPSC-CMs do not manifest arrhythmias but mutants FLNC and isogenic FLNC$^{KO-/-}$ iPSC-CMs display delayed afterdepolarizations indicated by the red arrows. (**F**) Percentage of proarrhythmic cells were higher in patient-derived and FLNC$^{KO-/-}$ iPSC-CMs. KO, knockout; ns, not significant. *$P < 0.05$, **$P < 0.01$, ***$P < 0.001$, and ****$P < 0.0001$.

The PDGFRA is up-regulated in FLNC-related cardiomyopathy and a downstream regulator of β-catenin

To identify a more downstream target for drug discovery, we compared the transcriptomes from *FLNC*$^{KO-/-}$ and *FLNC*$^{KO+/-}$ with isogenic iPSC-CMs to identify potential target genes that are associated with FLNC haploinsufficiency in DCM. We observed that both *FLNC*$^{KO-/-}$ and *FLNC*$^{KO+/-}$ iPSC-CMs had approximately equal numbers of up-regulated and down-regulated DEGs, with *FLNC*$^{KO-/-}$ having higher (by 10%) up-regulated DEGs compared to *FLNC*$^{KO+/-}$ iPSC-CMs (58.9%; *FLNC*$^{KO-/-}$ versus 49.9%; *FLNC*$^{KO+/-}$ DEGs) (Fig. 4A).

Downloaded from https://www.science.org at Universita degli Studi di Trieste on March 30, 2022

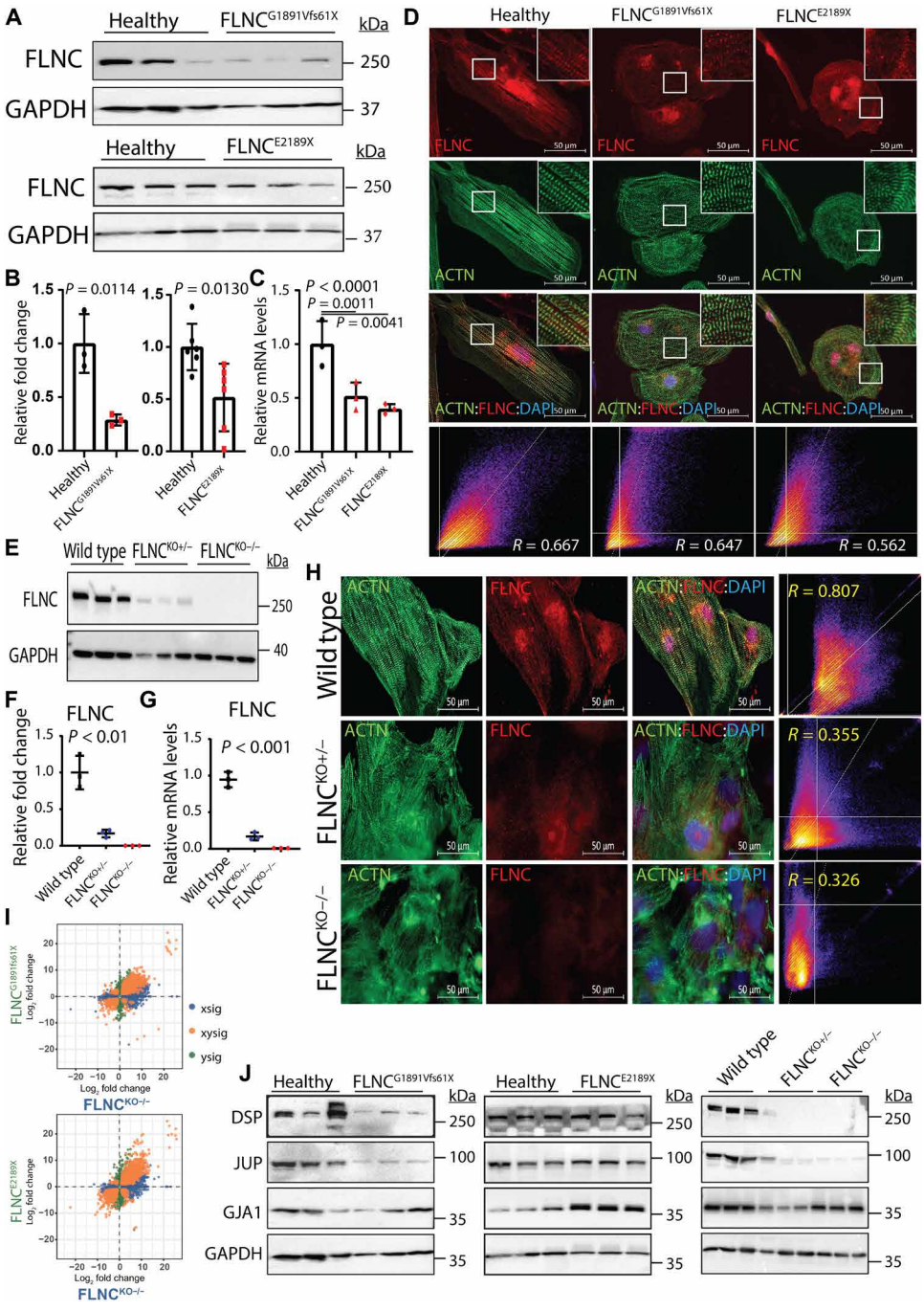

Fig. 2. FLNC^{G1891Vfs61X} and FLNC^{E2189X} are loss-of-function mutations leading to haploinsufficiency in FLNC-related cardiomyopathy. (**A**) Expression levels of FLNC in patient-derived iPSC-CMs were significantly decreased as detected by immunoblot. (**B**) Quantitative representation of the immunoblots in (A). (**C**) FLNC mRNA expression levels were significantly decreased in patient-derived iPSC-CMs. (**D**) Detection of FLNC (red) by immunofluorescence staining in control and patients' iPSC-CMs, α-actinin (green), a cardiac myocyte marker, and 4′,6-diamidino-2-phenylindole (DAPI)–stained (blue). FLNC was colocalized with ACTN by ImageJ colocalization analysis. (**E**) FLNC expression levels were significantly decreased by immunoblots in heterozygous and homozygous KO iPSC-CMs. (**F**) Quantitative representation of the immunoblots from (E). (**G**) FLNC mRNA expression levels were significantly decreased in FLNC heterozygous and homozygous KO iPSC-CMs compared to isogenic controls. (**H**) Significantly reduced detection of FLNC (red) at Z-disc (green) and confirmed by ImageJ colocalization analysis. (**I**) DEGs from patients' iPSC-CMs were highly concordant with FLNC homozygous KO iPSC-CMs. (**J**) FLNC-deficient iPSC-CMs affected expression levels of intercalated disc proteins. All experiments were independently repeated three times. DSP, desmoplakin; JUP, plakoglobin; GAPDH, glyceraldehyde-3-phosphate dehydrogenase.

Downloaded from https://www.science.org at Universita degli Studi di Trieste on March 30, 2022

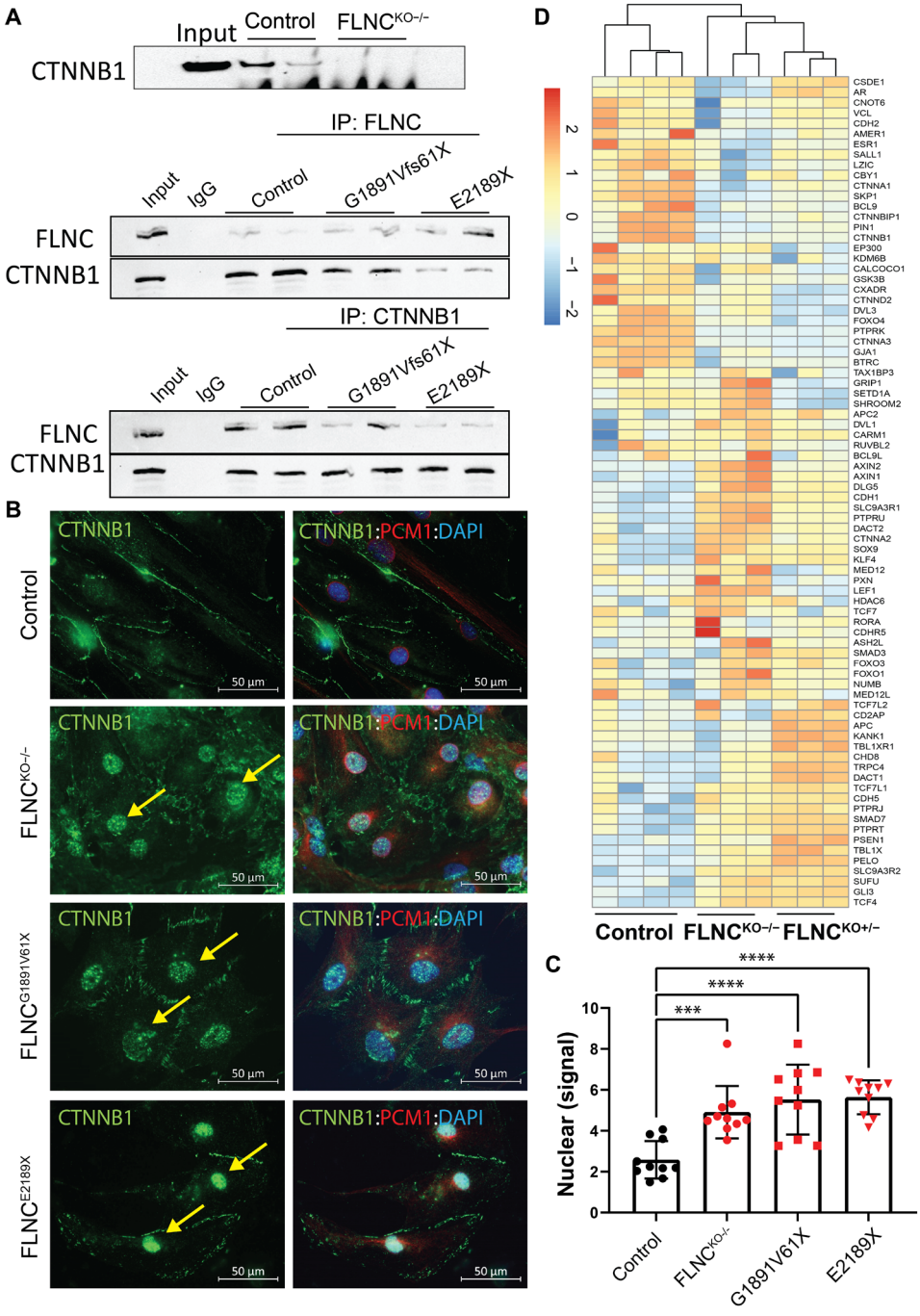

Fig. 3. β-Catenin is associated with FLNC and the loss of the FLNC-activated β-catenin signaling pathway. (**A**) β-Catenin was not detected in the coimmunoprecipitation pull-down lysate from FLNC KO iPSC-CMs. Each lane represents one differentiation batch. There is a reduction in the amount of β-catenin in the pull-down protein lysate from patients' iPSC-CMs using antibody against FLNC. Each lane represents one iPSC-CM immunoprecipitation (IP) sample. IP: FLNC, IP with FLNC antibody; IP: CTNNB1, IP with coimmunoprecipitation and proteomic analysis identified β-catenin antibody. (**B**) Immunofluorescence staining against active β-catenin (green) showed increased nuclear localization of β-catenin in FLNC homozygous KO and patients' iPSC-CMs. PCM1 (red) is a marker of cardiac myocytes. Nuclei (blue) was stained with DAPI. Yellow arrows indicate nuclear localization of β-catenin. All experiments were independently repeated three times. (**C**) Quantification of nuclear vs cytoplasmic CTNNB1 from the IF images in Fig. 3C. (D) Heatmap plot of DEGs involved in the β-catenin signaling pathway indicating β-catenin signaling activation in FLNC KO lines. PCM, pericentriolar material 1.

Notably, the dysregulated genes from the FLNC homozygous and heterozygous genotypes were highly concordant (fig. S8). Therefore, we used up-regulated (1498 genes) and down-regulated (1284 genes) DEGs that were shared between homozygous and heterozygous for more in-depth pathways and functional enrichment analyses. The analyses revealed that up-regulated genes were enriched in Kyoto Encyclopedia of Genes and Genomes pathways involved in regulating cell-cell adhesion, intercellular communication, and ion transport (Fig. 4, B and C) as evidenced by the expression heatmap shown in Fig. 4D. Moreover, the up-regulated genes were found to be

Downloaded from https://www.science.org at Universita degli Studi di Trieste on March 30, 2022

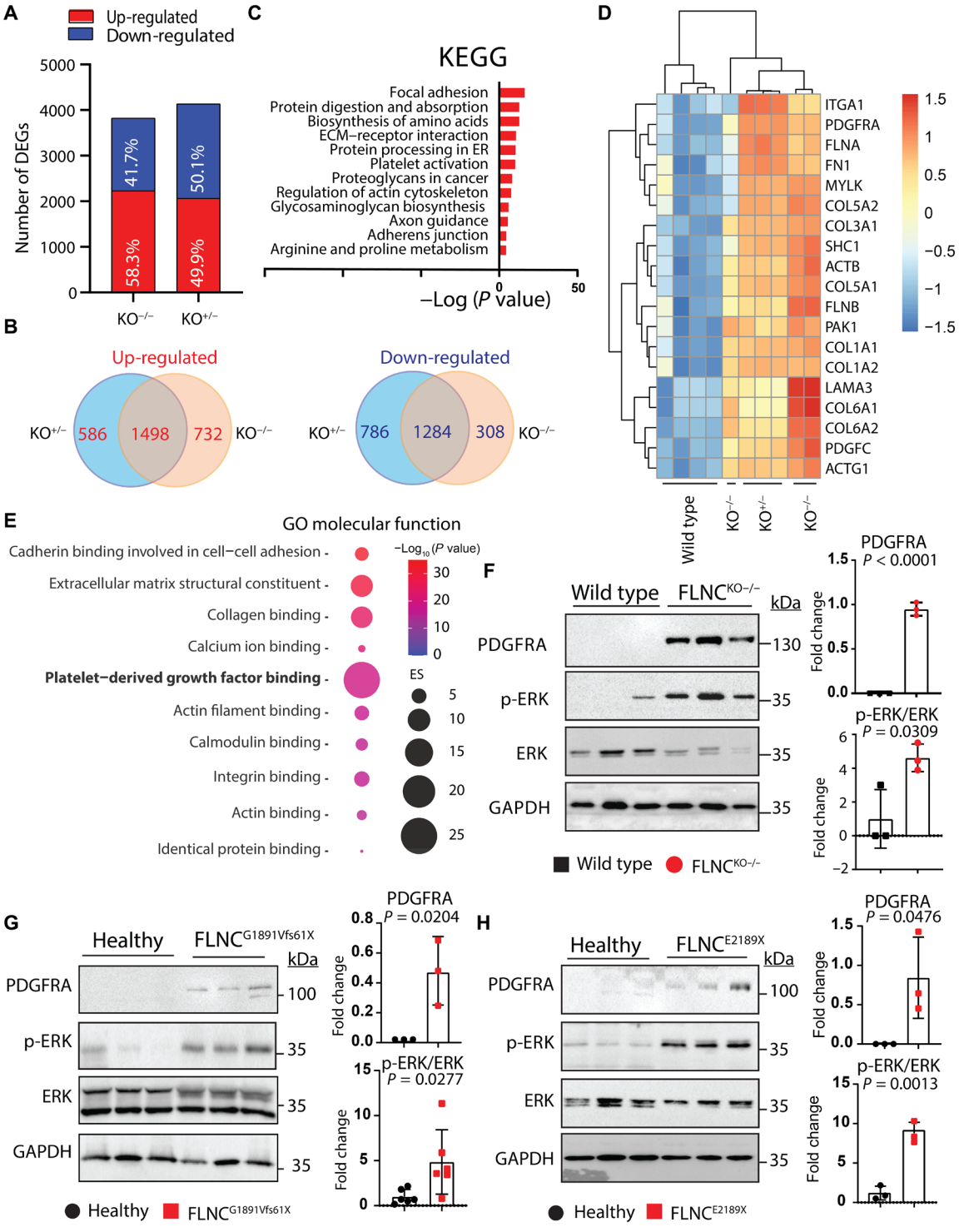

Fig. 4. Dysregulation of cell-cell adhesion pathways resulted in PDGFRA activation in the pathogenesis of FLNC-related cardiomyopathy. (**A**) Number of DEGs in FLNC heterozygous and homozygous KO iPSC-CMs compared to isogenic control iPSC-CMs. Percentage representation of the DEGs for each line is listed as up-regulated (red) and down-regulated (blue) in the bar graphs. (**B**) Venn diagram of shared DEGs between FLNC heterozygous and homozygous iPSC-CMs. (**C**) Enrichment analysis of Kyoto Encyclopedia of Genes And Genomes (KEGG) datasets identified dysregulation of pathways involved in cell-cell adhesion systems and membrane signaling. ECM, extracellular matrix. ER, Endoplasmic Reticulum. (**D**) Heatmap of DEGs in dysregulated cell-cell adhesion pathway (hsa04510). (**E**) GO analysis of DEGs revealed activation of the PDGF signaling pathway. Color codes indicate $\log_{10}$ transformed *P* values of the top 10 dysregulated pathways in GO molecular function. The number of genes involved in each pathway is represented by the size of the bubble. (**F** to **H**) PDGFRA and phosphorylated extracellular signal–regulated kinase (p-ERK) expression levels were significantly up-regulated in FLNC KO and patient's iPSC-CMs as detected by immunoblot. Quantitative representation of each blot was presented as dot plots. All experiments were independently repeated three times.

Downloaded from https://www.science.org at Universita degli Studi di Trieste on March 30, 2022

enriched in PDGF binding activities at the molecular levels with the highest enrichment score in *FLNC* KO iPSC-CMs compared to the isogenic controls' iPSC-CMs (Fig. 4E). The activation of PDGFR pathway suggested by the transcriptome analysis was confirmed by detection of increased protein levels of PDGFRA by immunoblotting. Also, we checked on an additional FLNC homozygous KO clone and observed the same PDGFRA up-regulation (fig. S9). The data showed that PDGFRA expression levels were markedly increased by fourfold in *FLNC* KO lines compared to isogenic control iPSC-CMs (Fig. 4F). Since our data suggest that $FLNC^{G1681Vfs61X}$ and $FLNC^{E2189X}$ mutations cause haploinsufficiency, we hypothesized that PDGFRA levels may be increased also in the patients' iPSC-CMs carrying these mutations. As shown in Fig. 4 (G and H), PDGFRA was up-regulated in both lines of patient-derived iPSC-CMs compared to control iPSC-CMs. Together, the findings suggest that the activation of PDGFRA signaling pathway is implicated in the pathogenesis of FLNC-related cardiomyopathy.

β-Catenin has been suggested to up-regulate expression of PDGFRA in other tissues and/or diseases (*29*–*31*). Because of our observation of significant nuclear localization of β-catenin in FLNC-deficient iPSC-CMs, we investigated the hypothesis that β-catenin is an upstream transcription activator of PDGFRA. Hence, we inhibited β-catenin using β-catenin inhibitors (JW67 and JW74) at different concentrations and observed a dose-dependent suppression of the PDGFRA transcript levels (Fig. 5A). Moreover, the chromatin immunoprecipitation (ChIP) pull-down experiment showed that SOX2, a known transcription factor and a β-catenin binding partner, binds to the *PDGFRA* promoter region (Fig. 5B). Together, the data suggest that β-catenin is likely a transcriptional activator of PDGFRA and that nuclear localization of β-catenin causes sustained up-regulation of PDGFRA in FLNC-deficient iPSC-CMs.

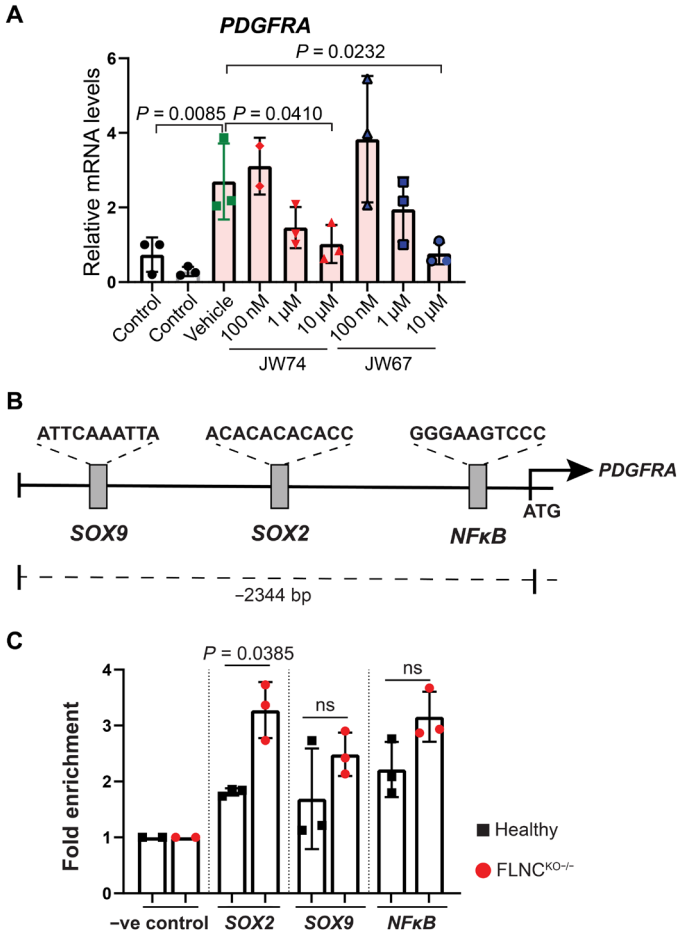

Fig. 5. β-Catenin is a possible transcription activator of PDGFRA. (**A**) Dosage-dependent decrease of PDGFRA mRNA levels upon inhibition of β-catenin using JW67 and JW76. All experiments were independently repeated three times. (**B**) In silico analysis of transcription factors binding sites on PDGFRA regulatory region. (**C**) Chromatin immunoprecipitation polymerase chain reaction (qPCR) showed enrichment of β-catenin–*SOX2* binding to the promoter region of *PDGFRA*. NFκB, nuclear factor κB.

PDGFRA inhibition rescued connexin 43 membrane localization

PDGFRA is known to disrupt connexin 43 [Gap junction protein alpha-1 (GJA1)] communication at the cell membrane through activation of MAPK/extracellular signal–regulated kinase (ERK) signaling (*32*–*35*). Several studies have shown that MAPK/ERK signaling activation induces phosphorylation of GJA1, which leads to its internalization and, subsequently, disruption of the gap junction function (*36*–*38*). GJA1 dysfunction in the heart has also been found to hamper contractility and induce arrhythmias (*39*–*41*). Our data revealed activation of ERK, a MAP kinase, and GJA1 mobilization away from the cell membrane in FLNC mutant and KO iPSC-CMs compared to control iPSC-CMs (Fig. 6A). To test that PDGFRA activation in our FLNC haploinsufficient iPSC-CMs is responsible for mislocalization of GJA1, we pharmacologically inhibited PDGFRA with crenolanib, a U.S. Food and Drug and Administration (FDA)–approved drug, to determine the effects on GJA1 membrane localization. PDGFRA inhibition by crenolanib rescued GJA1 localization to the membrane as shown by an immunofluorescence study (Fig. 6A).

The transcriptome analysis revealed that $FLNC^{E2189X}$ mutant iPSC-CMs showed the greatest response to crenolanib with the highest number of rescued DEGs as compared with the $FLNC^{G1891Vfs61X}$ mutant and the KO iPSC-CMs (Fig. 6B). Notably, Gene Set Enrichment Analysis (GSEA) revealed partial normalization of the cell adhesion pathway (hsa04510), supporting the hypothesis that structural stabilization of the cell-cell adhesion sites facilitated GJA1 attachment on the cell membrane (Fig. 6C and fig. S10). Nevertheless, we found that GJA1 expression levels were not altered upon treatment with crenolanib as detected by immunoblotting, suggesting that PDGFRA inhibition does not affect expression levels but rather affects GJA1 trafficking (Fig. 6D and fig. S11). Last, and critically, treatment with crenolanib also significantly improved the contractility and reduced arrhythmias in iPSC-CMs derived from patients with FLNC, but not healthy control individuals (Fig. 6, E and F, and figs. S12 and S13). This beneficial effect was specific to PDGFRA inhibition, as we did not observe any rescuing effect after treatment with ERK or other tyrosine kinase inhibitors (TKIs) (fig. S14 to S17). Hence, our data suggest that PDGFRA inhibition partially restored membrane localization of GJA1, which may contribute to improvement in cardiac contractility and the electrical stability in iPSC-CMs derived from patients with *FLNCtv*.

PDGFRA inhibition blunted nuclear localization of β-catenin

We detected increased nuclear localization of β-catenin in FLNC mutant iPSC-CMs by immunofluorescence, compared to control iPSC-CMs (Fig. 7A). Upon crenolanib treatment, we observed a

Downloaded from https://www.science.org at Universita degli Studi di Trieste on March 30, 2022

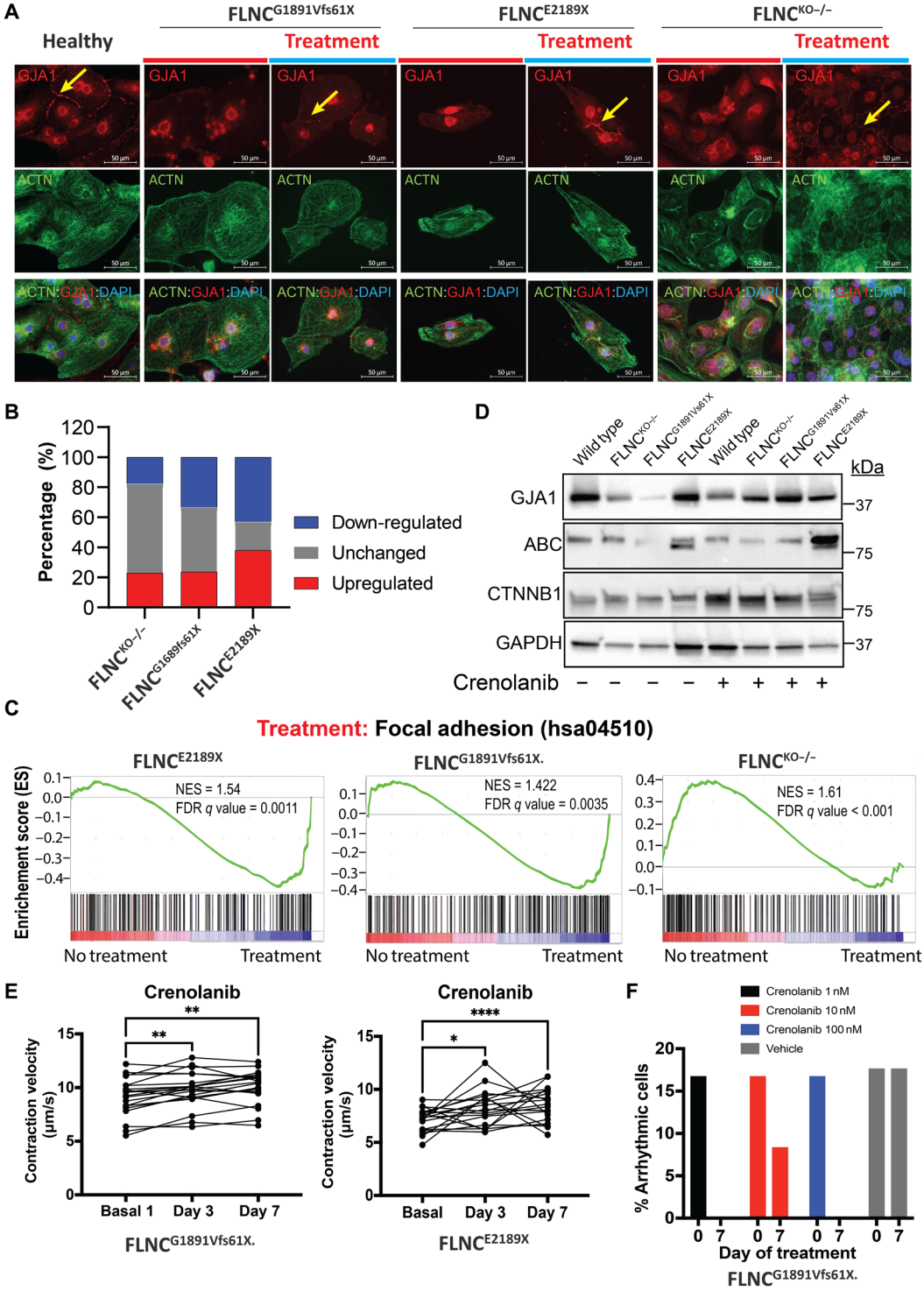

Fig. 6. The loss of FLNC causes dysregulation to the cell-cell adhesion systems and inhibition of PDGFR signaling improved contractility of FLNC mutant iPSC-CMs. (**A**) Immunofluorescence staining evidenced the loss of FLNC that resulted in segregation of GJA1 (red) away from the membrane compared to control iPSC-CMs. GJA1 segregated at the membrane upon treatment with crenolanib. α-Actinin was stained in green as a marker for Z-disc and cardiomyocytes. Nuclei (blue) were stained with DAPI. Yellow arrows indicate membrane localization of GJA1. (**B**) FLNC^{E2189X} iPSC-CMs had the largest DEGs changes to the cell adhesion pathway compared to other FLNC-mutant lines upon crenolanib treatment. (**C**) Gene Set Enrichment Analysis (GSEA) indicated partial normalization of the cell adhesion pathway upon treatment with crenolanib in patients' and FLNC KO iPSC-CMs. (**D**) Immunoblots indicated no significant changes to expression levels of GJA1, active β-catenin, and total β-catenin before and after PDGFRA inhibition. All experiments were independently repeated three times. (**E**) PDGFRA inhibition improved contractility of patients' iPSC-CMs. (**F**) Crenolanib treatment over a period of 7 days showed improved contractility of patients' iPSC-CMs ($n = 20$ repeated measured replicates). *$P < 0.05$, **$P < 0.01$, and ****$P < 0.0001$.

Downloaded from https://www.science.org at Universita degli Studi di Trieste on March 30, 2022

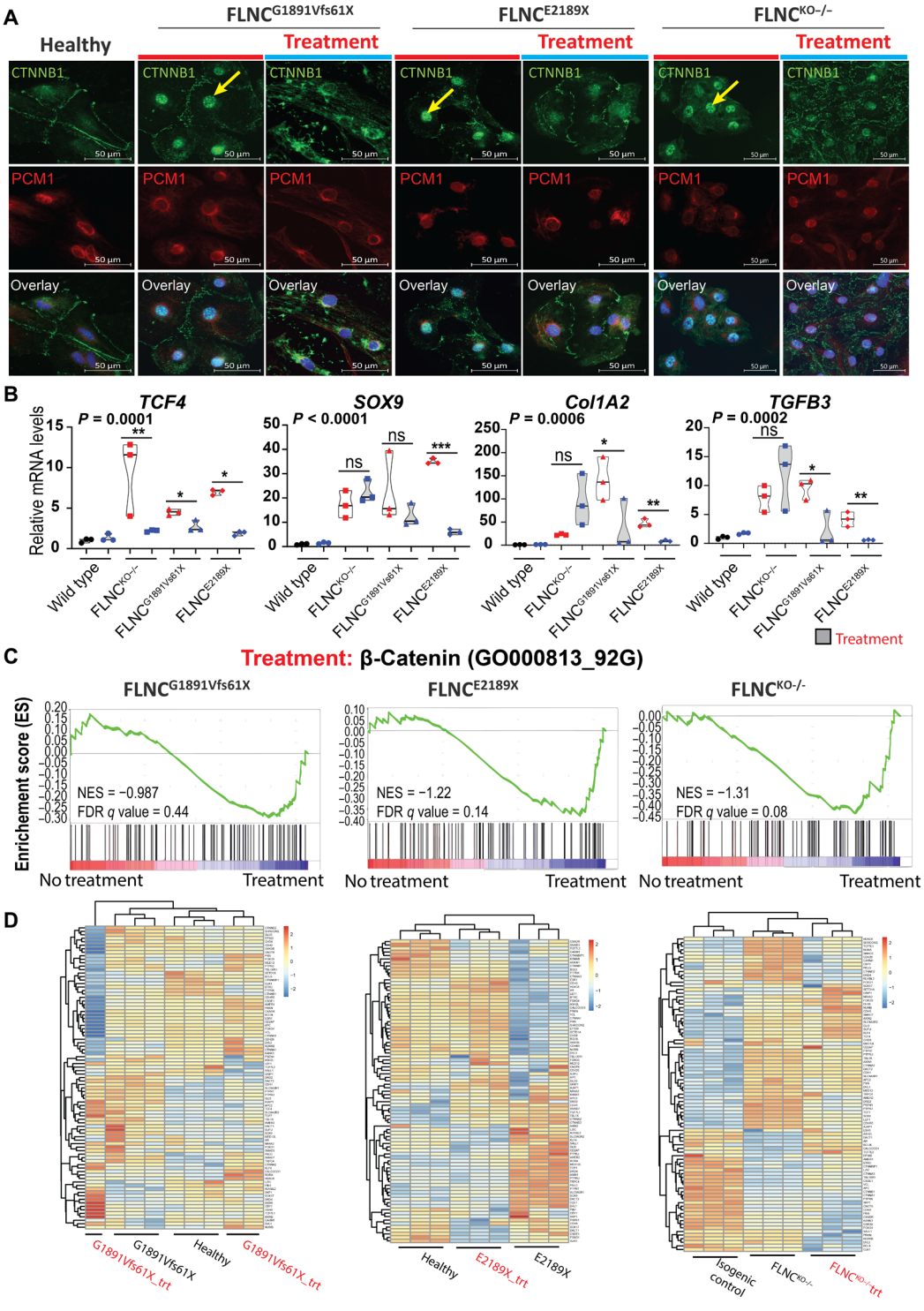

Fig. 7. PDGFRA inhibition attenuated β-catenin signaling and its nuclear localization in FLNC mutant iPSC-CMs. (**A**) Immunofluorescence staining against active β-catenin (green) showed increased nuclear localization of β-catenin in FLNC homozygous KO and patients' iPSC-CMs. PCM1 (red) is a marker of cardiac myocytes. Nuclei (blue) were stained with DAPI. Treatment with crenolanib prevented nuclear localization of β-catenin in FLNC homozygous and patients' iPSC-CMs. Yellow arrows indicate nuclear localization of β-catenin. (**B**) Reduced β-catenin targets transcripts by qPCR in FLNC mutant lines. (**C**) GSEA analysis showed partial normalization of the β-catenin signaling pathway in FLNC mutant lines. (**D**) Heatmaps showing partial normalization of expression profiles in genes involved in β-catenin signaling in FLNC mutant iPSC-CMs. ns, not significant. *P < 0.01, **P < 0.001, and ***P < 0.0001. All experiments were independently repeated three times.

Downloaded from https://www.science.org at Universita degli Studi di Trieste on March 30, 2022

significant decrease in β-catenin nuclear location in both FLNC mutant and FLNC KO iPSC-CMs compared to control iPSC-CMs (Fig. 7A). The beneficial inhibitory effects of crenolanib on β-catenin nuclear signaling were confirmed by qPCR, which showed reduced expression of the transcript levels of β-catenin targets genes, such as *TCF4*, *SOX9*, *COL1A2*, and *TGFβ3* (Fig. 7, A and B). Moreover, when we compared the profile of DEGs in patient-derived and KO iPSC-CMs before and after crenolanib treatment by GSEA analysis, we further confirmed partial rescue of the β-catenin signaling pathway after suppression of PDGFRA signaling (Fig. 7C and figs. S18 and S19). The finding is also supported by the normalization of the DEGs involved in the β-catenin signaling as shown in the heatmaps in Fig. 6D. The evidence therefore suggests that PDGFRA activation potentiates β-catenin signaling and promotes a positive feedback loop. Furthermore, we demonstrated that PDGFR inhibition can partially restore β-catenin membrane localization, reducing its activation caused by *FLNCtv* mutations.

PDGFRA signaling activation in a-DCM

To confirm the findings from the in vitro studies, we determined the PDGFRA expression levels in the hearts of human patients with a-DCM. Among the patients with a-DCM ($n = 5$), one of the patients was the sister of the proband with the $FLNC^{G1891V61X}$ mutation. The other four patients were diagnosed with idiopathic DCM with ventricular arrhythmias. We found that PDGFRA levels were increased in the heart of the patients with a-DCM. We also showed that the PDGFRA downstream effector, ERK, was activated as shown by the increased levels of its phosphorylated form (Fig. 8, A and B). Also, we determined the expression levels and localization of β-catenin and GJA1 in the DCM hearts. Although the expression levels of β-catenin and GJA1 remained unchanged as shown by immunoblotting, β-catenin and GJA1 were dissociated from the cell membrane as detected by immunofluorescence staining (Fig. 8, C to E). Moreover, the RNA-seq data from explanted hearts showed significantly higher PDGFRA mRNA abundance in the hearts of a-DCM ($n = 20$) compared to DCM ($n = 15$) and nonfailing hearts ($n = 12$) (Fig. 8F). The RNA-seq data were confirmed by qPCR as shown in Fig. 8G. Moreover, PDGFRB mRNA transcript levels were not changed among groups, suggesting that the pathogenic mechanisms of a-DCM caused by FLNC mutations are specific to the PDGFRA isoform (Fig. 8F). In summary, we confirmed the in vitro findings from patient-specific and KO iPSC-CM lines and from human a-DCM explanted hearts, strongly suggesting that PDGFRA promotes pathogenic signaling in a-DCM.

DISCUSSION

FLNC is a known actin cross-linker with an important role in structural integrity of Z-discs, IDs, and cell membranes (*42*, *43*). In our study, we found that β-catenin is the downstream target of FLNC and that FLNC haploinsufficiency not only affects cell-cell adhesion, and cytoskeletal and sarcomeric organization, but also increased nuclear migration of β-catenin that, in turn, up-regulates transcription of PDGFRA. The consequent activation of PDGFRA signaling is likely responsible for the contractile dysfunction and electrical instability observed in FLNC mutant iPSC-CMs. The arrhythmic phenotype caused by FLNC haploinsufficiency and subsequent PDGFRA activation is at least partly due to displacement of GJA1 from the cell membrane induced by several mechanisms, such as phosphorylation by the PDGFRA downstream target ERK, ID disruption, and abnormal translocation due to disorganization of the cytoskeleton network.

Moreover, we show an attenuation of the arrhythmic phenotype of FLNC patients' iPSC-CMs by inhibiting the PDGFRA signaling using crenolanib, an FDA-approved PDGFRA inhibitor. The findings identify PDGFRA as a potential preventive and therapeutic target in FLNC-related cardiomyopathies caused by FLNC haploinsufficiency and imply that FDA-approved PDGFRA inhibitors could be repurposed to treat these specific cardiomyopathies (Fig. 9).

Plakophilin-2, desmoplakin, desmoglein-2, desmocolin-2, and plakoglogin encoding desmosomal proteins are important for ID formation and signaling transduction in cardiomyocytes (*44*–*47*) and are the most commonly mutated genes in ACM (*48*), suggesting that disruption in cell-cell adhesion and activation of the subsequent signaling cascades contribute to arrhythmias and heart failure in ACM. As FLNC is important in maintaining the membrane structure and mechano-transduction (*9*, *49*), it is anticipated that mutations in this gene will disrupt the dynamic of the adhesion junctions and signaling, resulting in contractile dysfunction and arrhythmias. This hypothesis is supported by studies in FLNC KO mouse hearts (*50*), as well as by our findings in patient-specific and FLNC KO iPSC-CMs. Since it would be difficult to reverse structural disruption of IDs without gene therapy, this study aimed to identify the signaling pathways affected by *FLNC* truncating mutations that contribute to disease development. Our findings also provide insights into understanding the disease mechanism related to desmosome or cadherin dysfunction in which cell-cell adhesion is similarly affected.

By examining the changes of the FLNC interactome in patient-specific iPSC-CMs, we identified β-catenin and hypothesized that FLNC is important in retaining β-catenin at the cell membrane for signal transduction. We found that, in both FLNC patient iPSC-CM lines, β-catenin was localized in the nucleus and β-catenin signaling was activated as indicated by up-regulation in the expression of target genes. Although our findings are consistent with the notion that β-catenin is implicated in ACM where cardiac-specific ablation of plakoglobin results in activation of β-catenin signaling (*51*), it is not clear how the loss of FLNC affects the stability of β-catenin and its nuclear localization in FLNC-related cardiomyopathy. Under normal physiological conditions, β-catenin that is not membrane-bound is rapidly destroyed by the β-catenin destruction complex, preventing its nuclear translocation and formation of the TCF/LEF DNA transcription complex responsible for the transcription of its gene targets (*52*–*54*). In our study, the transcriptome profile of FLNC KO iPSC-CMs indicated activation of cadherin binding (by GO analysis) (Fig. 4E). This finding is in line with several studies showing that activation of β-catenin is associated with up-regulation of cadherin transcription levels. Our findings and those of others suggest a negative feedback loop in which β-catenin could up-regulate cadherins, which, in turn, inhibit β-catenin signaling by sequestering β-catenin at the cell membrane to prevent its nuclear localization (*55*–*59*). Moreover, cadherin dysregulation has been shown to cause ID remodeling in the heart (*60*, *61*). Together, our data suggest a possible role of FLNC in the formation of cadherin/β-catenin complex in regulating cell-cell adhesion and in attenuation of β-catenin signaling in cardiomyocytes.

However, the compounds JW67 and JW74, which facilitate β-catenin destruction and hence inhibit Wnt signaling, failed to

Downloaded from https://www.science.org at Universita degli Studi di Trieste on March 30, 2022

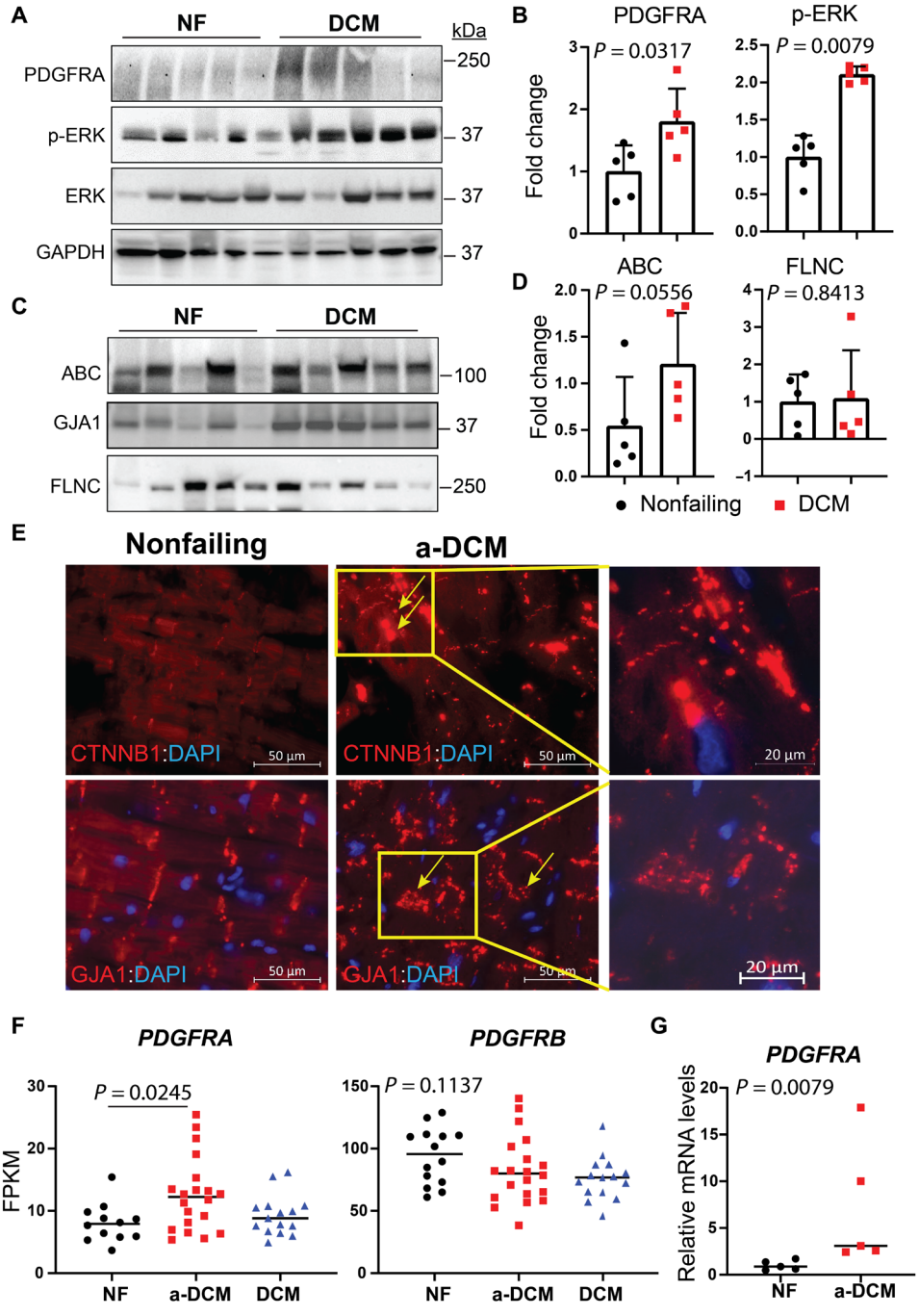

Fig. 8. Up-regulation of PDGFRA contributes to GJA1 and β-catenin delocalization in the hearts of arrhythmogenic dilated cardiomyopathy. (**A**) Up-regulation of PDGFRA and its effector p-ERK expression levels in the hearts of patients with a-DCM compared to nonfailing (NF) hearts ($n = 5$). (**B**) Quantitative representation of the immunoblots in (A). (**C**) Active β-catenin expression levels were not significantly different compared to NF hearts ($n = 5$). (**D**) Quantitative representation of the immunoblots in (C). (**E**) RNA-seq data showing up-regulation of PDGFRA transcripts but not PDGFRB in the hearts of a-DCM compared to DCM and NF. (**F**) Validation of increased PDGFRA transcripts observed in (E) by qPCR. (**G**) Immunofluorescence staining against CTNNB1 (red) and GJA1 showed CTNNB1 and GJA1 mobilized away from the ID of cardiac myocytes in the hearts of a-DCM compared to NF. Nuclei (blue) were stained with DAPI. Yellow arrows indicate GJA1 and β-catenin segregated away from the cell membrane. All experiments were independently repeated three times. ABC, Active beta-catenin.

confer any functional rescue in FLNC patient–derived iPSC-CMs, suggesting that β-catenin may be too upstream to have a substantial role in the pathogenesis of FLNC-related cardiomyopathy. JW67 and JW74 reduce β-catenin levels rather than prevent its nuclear localization, and our data demonstrated that FLNC deficiency did not change expression levels of β-catenin but rather affected nuclear and cytoplasm distribution of β-catenin (Fig. 6, A and D).

By profiling the transcriptomes of FLNC patient and FLNC KO iPSC-CMs, we identified PDGFRA as a potential disease pathway that is downstream of β-catenin. Our findings on ERK activation

Downloaded from https://www.science.org at Universita degli Studi di Trieste on March 30, 2022

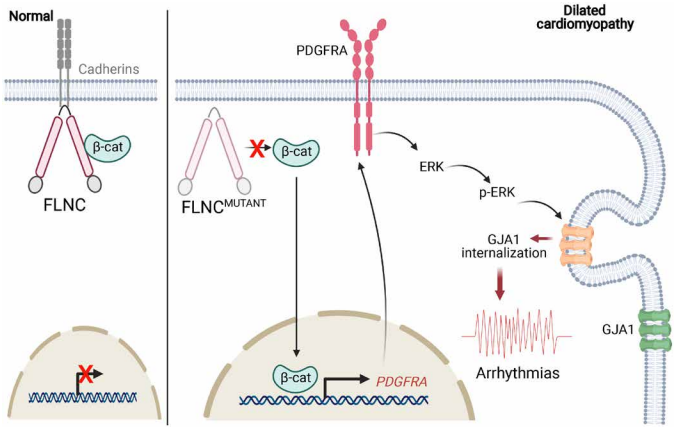

Fig. 9. Disease model of FLNC-related cardiomyopathy. Our data indicate that β-catenin (β-cat) localized to the cell membrane with FLNC in the NF hearts (left). However, the loss of FLNC perturbed the cytoplasmic β-catenin and increased nuclear localization of β-catenin and activates transcription of PDGFRA, which leads to sustained up-regulation of PDGFRA signaling at the cell-cell membrane and, subsequently, activation of ERK signaling resulting in internalization of GJA1 and consequently arrhythmias in the heart of patients with a-DCM (right).

and GJA1 mislocalization are also consistent with an activated PDGFRA signaling in patient iPSC-CMs. It is known that, in healthy cardiomyocytes, PDGFRA expression is very low (*62*, *63*). Thus, increased PDGFRA levels in FLNC haploinsufficiency may serve as a disease-specific marker, as well as a feasible therapeutic target. When we inhibited PDGFRA by treating the cells with crenolanib, GJA1 membrane localization was restored for proper gap junction formation, which partly explains the reduction in arrhythmia observed in patients' iPSC-CMs. It should be noted that only PDGFRA inhibition was able to mediate rescuing effects, while treatment with β-catenin inhibitors or ERK antagonists failed to exert the same beneficial effects, possibly due to their nonspecific effects on multiple downstream subcellular substrates. Hence, our findings indicate that PDGFRA pathway activation is central and specific to the pathogenesis of FLNC-related cardiomyopathy.

We observed that PDGFRA pharmacological inhibition could effectively reduce β-catenin nuclear translocation, suggesting that β-catenin–PDGFRA signaling constitutes a positive feedback loop that may exacerbate the disease progression. Instead of blocking β-catenin activity, it would be more advantageous to prevent its pathological nuclear translocation in the absence of FLNC as this strategy will not affect β-catenin signaling function that is necessary for several important physiological processes in iPSC-CMs. Moreover, the β-catenin inhibitors JW67 and JW74 have been shown to reduce cytoplasmic levels of β-catenin (*64*); hence, we hypothesize that lack of cytoplasmic β-catenin could further disrupt the adhesion systems of FLNC mutant iPSC-CMs. However, additional studies are required to understand how PDGFRA inhibitor blunted nuclear localization of β-catenin in cardiac myocytes. Cancer studies have shown that activation of PI3K/AKT signaling modulates β-catenin nuclear translocation; hence, it is highly probable that the PDGFRA inhibitor crenolanib reduces PI3K/AKT signaling, preventing nuclear localization of β-catenin in FLNC-deficient iPSC-CMs (*65*, *66*). Alternatively, PDGFR inhibition may reduce GSK3β phosphorylation by AKT and prevent degradation of β-catenin, which is consequently sequestered in the cytoplasm. As shown in Fig. 6D, the total expression of β-catenin was not changed in FLNC mutant and KO iPSC-CMs, indicating that the loss of FLNC perturbed the distribution of cytoplasm and nuclear pool of β-catenin rather than the levels of β-catenin. Moreover, in our study, RNA-seq and immunoblotting showed that expression levels of GJA1 were not changed at the mRNA and protein levels, suggesting that inhibition of PDGFRA rescued GJA1 internalization, likely by normalizing the ERK signaling (*67*). In summary, PDGFRA inhibition is beneficial to attenuate disease phenotype caused by FLNC haploinsufficiency in iPSC-CMs, due to its pivotal role in regulating both the β-catenin and GJA1 cellular localization. Moreover, the more downstream location of this target would largely translate into a more specific, less biological disruptive therapeutic effect. Therefore, further studies are warranted to identify mechanism-based targets specific to PDGFRA signaling to repurpose FDA-approved PDGFRA inhibitors in treating FLNC-related cardiomyopathy.

Notably, PDGFR inhibition may appear to be a viable strategy in treating ACM in general. Compared to healthy and DCM hearts, PDGFRA transcript levels were higher in a-DCM samples than in samples from DCM without arrhythmic burden, indicating that PDGFRA activation may be a specific signature of increased arrhythmic risks in cardiomyopathies. It has been reported that PDGFRB is induced in LMNA-related ACM, further suggesting the therapeutic potential of PDGFR family inhibition in treating arrhythmogenic cardiac diseases (*22*). However, PDGFRB was not up-regulated in our a-DCM patient samples, suggesting that induction of the PDGFRB isoform may be specific to *LMNA* mutations; alternatively, it is possible that we did not find increased expression of PDGFRB transcripts that were masked by small number of hearts with *LMNA* mutations in our heart tissue pool. Nevertheless, our data and published data highlight the importance of a future meta-study to assess the specificity of PDGFR signaling in arrhythmogenic cardiomyopathies.

Crenolanib is a TKI used for the treatment of various types of cancer. TKIs are known to induce cardiovascular side effects (*68*). In this regard, determining the optimal dose of this drug in patients with a-DCM will be the key to maximize the clinical benefits and reduce the side effects. Previous TKI toxicity studies using iPSC-CMs, iPSC-endothelial cells, and iPSC-cardiac fibroblasts have shown that TKIs in general are toxic at concentrations higher than 1 μM (*69*, *70*). On the basis of our findings, 1 μM crenolanib conferred cardiac function improvement without compromising cardiomyocyte survival (fig. S20), which is consistent with previously published findings on LMNA iPSC-CMs (*22*). The data suggest that the low dose of a PDGFR inhibitor may be effective in treating FLNC-related cardiomyopathy without provoking cardiovascular adverse effects. Conducting a more extensive study, using multiple lines of iPSC cell derivatives to examine the cardiac safety index and the effective therapeutic window will be instrumental to examine the feasibility of PDGFR inhibition as a therapeutic strategy to treat cardiac diseases (*71*). Another caveat is that crenolanib can also inhibit other tyrosine kinases (*72*). Future studies are warranted to examine whether the protective or toxic effects of crenolanib may be mediated through other tyrosine kinases.

In summary, using patient-specific iPSC-CMs to reveal the disease-specific mechanism of FLNC-related cardiomyopathy, we identified a novel link to β-catenin and PDGFRA that could potentially be important therapeutic targets. We show that treatment with crenolanib, a PDGFRA inhibitor, can partially reverse the

Downloaded from https://www.science.org at Universita degli Studi di Trieste on March 30, 2022

pathological gene expression profile, cardiac dysfunction, and electrical instability in FLNC patient–specific cardiomyocytes. Our novel findings open the way to further mechanistic studies to understand the role of PDGFRA pathways in the pathogenesis of arrhythmogenic cardiomyopathies and to test the feasibility of PDGFRA inhibition as a strategy for long-term disease management.

MATERIALS AND METHODS

Study populations

Patients with FLNC mutations were selected from the Familial Cardiomyopathy Registry (COMIRB 99-177), a multicenter, three-decade-long ongoing project studying human hereditary cardiomyopathies from University of Colorado and University of Trieste hospitals. The 1999 consensus criteria of the Guidelines for Familial Dilated Cardiomyopathy were used to diagnose patients with DCM (*73*). Detailed medical history, physical examination, and clinical testing were performed and recorded at baseline and during follow up, as previously reported (*74*). Patients with DCM were identified based on the presence of left ventricular fractional shortening <25% and/or an ejection fraction <45%, and left ventricular end-diastolic diameter >117% of the predicted value. ARVC diagnosis was based on the 2010 ARVC Task Force Criteria (*75*). Informed consent forms were obtained from each patient according to the institutional review boards. Blood samples were collected from consented individuals, and genomic DNA was extracted using a commercial kit (Qiagen). Whole-exome sequencing (WES) was performed using the Illumina TruSight One Sequencing Panel. All genetic variants identified were confirmed by Sanger sequencing. Briefly, exomes of *FLNC* were amplified by PCR, and Sanger sequencing was performed using the Big Dye Terminator Cycle Sequencing Ready Reaction Kit on an ABI Genetic Analyzer 3730xl (Applied Biosystems) to determine the genetic codes. Genetic variants identified were confirmed in both sense and antisense directions in separate sequencing reactions when detected.

As previously described, patients with a-DCM are those with DCM who had a history of ventricular tachycardia requiring implantable cardioverter defibrillator placement and had at least one appropriate electric shock within 1 year before transplant (*76*). The patients with nonarrhythmogenic DCM had no report of ventricular tachycardia at any point throughout their medical history. Nonfailing were organ donors with no major cardiac history and a left ventricular echocardiography-based shortening fraction of ≥25% (*76*).

Ethical approval

The study protocol was approved by the local Institutional Review Board and was in accord with the Human Subjects' Committee guidelines. Informed consent forms were provided and signed by the study subjects.

Generation of iPSC deficient of FLNC using CRISRP-Cas9 system

Patient iPSCs were generated by the Stanford Cardiovascular Institute (Stanford CVI). $FLNC^{G1891Vfs61X}$ and $FLNC^{E2189X}$ are lines SCVI1116 and SCVI1115, respectively. Four healthy control lines were from the Stanford CVI (SCVI 113, SCVI 15, SCVI 202, and SCVI 273 are healthy 1, 2, 4, and 5, respectively). Healthy 3 is the commercially available iPSC line from WiCell. One clone was used for each line.

We performed genome editing on the commercial iPSC line using the CRISPR-Cas9 system from Integrated DNA Technologies Inc. (Coralville, Iowa). Briefly, ribonucleoprotein complexes were formed in vitro using CAS9 protein, guide RNA, and tracer RNA and delivered into iPSCs by electroporation. Next, the edited iPSCs were isolated from single-cell colonies to ensure homogeneity and the edited region/PAM site of FLNC was sequenced and validated by Sanger sequencing. One heterozygous KO line and two homozygous KO lines were studied.

Contractility analysis

iPSC-CM differentiation and contractility assessment were performed as previously described (*77*). Briefly, iPSC-CMs reseeded on Matrigel-coated 384-well plates were cultured for 7 days to recover their spontaneous beating. For comparison between various iPSC-CM lines, cell density was strictly controlled at 15,000 cells per well to avoid variations. Cardiomyocyte contraction was recorded with high-resolution motion capture tracking using the SI8000 Live Cell Motion Imaging System (Sony Corporation). During data collection, cells were maintained under controlled humidified conditions at 37°C with 5% CO_2 and 95% air in a stage-top microscope incubator (Tokai Hit). Functional parameters were assessed from the averaged contraction-relaxation waveforms from 10-s recordings, using the SI8000C Analyzer software.

Whole-cell patch-clamp recordings

Patch-clamp recordings were performed as previously described (*78*). iPSC-CMs were seeded on Matrigel-coated glass coverslips (Warner Instruments) for patch-clamp recordings. These recordings were conducted using an EPC-10 patch-clamp amplifier (HEKA). Glass pipettes with 3- to 4-megohm resistance were prepared using thin-wall borosilicate glass (A-M System) with a micropipette puller (Sutter Instrument). For recording, coverslips containing cardiomyocytes were transferred to a RC-26C recording chamber (Warner Instruments) mounted on the stage of an inverted microscope (Nikon). Spontaneous APs were recorded from cardiomyocytes superfused with Tyrode solution at 37°C (TC-324B heating system, Warner, USA). The Tyrode solution consisted of NaCl (140 mM), KCl (5.4 mM), $CaCl_2$ (1.8 mM), $MgCl_2$ (1 mM), Hepes (10 mM), and glucose (10 mM); pH was adjusted to 7.4 with NaOH. The pipette solution consisted of KCl (120 mM), $MgCl_2$ (1 mM), Mg-ATP (3 mM), Hepes (10 mM), and EGTA (10 mM); pH was adjusted to 7.2 with KOH. Data were acquired using PatchMaster software (HEKA) and digitized at 1.0 kHz. Data were analyzed using a custom-written MATLAB program.

Immunoblotting

iPSC-CMs were collected at 80 days and homogenized in radioimmunoprecipitation assay (RIPA) buffer (Pierce) containing 25 mM tris-HCl (pH 7.6), 150 mM NaCl, 1% NP-40, 1% sodium deoxycholate, and 0.1% SDS in the presence of protease inhibitor (Roche) and phosphatase inhibitors (Sigma-Aldrich). Frozen human ventricular tissues were homogenized in either RIPA buffer or in a lysis buffer containing 100 mM tris-HCl (pH 8.0), 0.2% SDS, 8 M urea, and 200 mM NaCl in the presence of protease inhibitor (Roche) and phosphatase inhibitors (Sigma-Aldrich).

The homogenates were centrifuged at 12,000 rpm for 10 min at 4°C, and the soluble lysates were used for experiments. Protein concentrations were measured by colorimetric RC DC protein assay (Bio-Rad). Aliquots of 30 μg of protein were denatured in a 5× Laemmli

Downloaded from https://www.science.org at Universita degli Studi di Trieste on March 30, 2022

buffer by boiling at 95°C for 5 min, separated on SDS–polyacrylamide gel electrophoresis, and transferred to nitrocellulose membranes. Target proteins were detected using specific primary antibodies (table S1), and the respective horseradish-linked secondary antibodies were used at concentrations recommended by the company. The ECL chemiluminescence system (Thermo Fisher Scientific) was used for signal amplification, and the signal was detected using the Bio-Rad ChemiDoc imaging system (Bio-Rad Laboratories). Glyceraldehyde-3-phosphate dehydrogenase (GAPDH) (Abcam) antibodies were used as loading controls.

Immunofluorescence staining

Paraffin-embedded ventricular samples were sectioned for immunofluorescence staining. Briefly, sections were deparaffinized using xylene. Subsequently, sections were rehydrated, transferred to 10 mM sodium citrate buffer (pH 6.0), and boiled for 15 min at 95°C for antigen unmasking. The slides were then cooled to room temperature and washed with phosphate-buffered saline (PBS). Subsequent steps were performed with reagents from a commercially available HRP-DAB Detection System (R&D Systems). The sections were blocked with blocking serum and incubated with primary antibody (table S1) at 4°C overnight. Samples were then washed in PBS and incubated with secondary antibody for 1 hour at room temperature. The sections were counterstained with 4′,6-diamidino-2-phenylindole and mounted with antifade mounting media (Richard-Allan Scientific). Images were taken using a Zeiss microscope equipped with a digital camera, and the stained area was quantified using ImageJ. Similar procedures, except for deparaffinization and rehydration, were carried out for iPSC-CM samples.

Coimmunoprecipitation

iPSC-CMs were lysed in 1× cell lysis buffer (Cell Signaling Technology), supplemented with protease inhibitor cocktail and phosphatase inhibitor cocktail (Thermo Fisher Scientific). The lysate was centrifuged at 5000 rpm for 3 min at 4°C. The centrifuged lysate was diluted to 1 g/liter (250 μl of final volume) and incubated with anti-FLNC (Atlas Antibodies), or immunoglobulin G antibody (Santa Cruz Biotechnology) at 4°C overnight with rotation. Twenty-five microliters of protein G PLUS agarose beads (Santa Cruz Biotechnology) was added into the mixture and incubated for an additional 5 hours. Agarose beads were sedimented and washed six times with the cell lysis buffer. Beads-bound proteins were dissociated in 2× SDS at room temperature for 30 min with vortexing at 5-min intervals. The identification of the associated proteins was determined by Western blots (table S1). Bead-bound proteins were also subjected to label-free–based quantitative proteomic analysis (Creative Proteomics).

Quantitative RT-PCR

RNA was extracted from iPSC-CMs or frozen ventricular tissue using a commercially available miRNeasy Mini Kit (QIAGEN, catalog no. 217006). Total RNA was treated with deoxyribonuclease 1 to remove genomic DNA (QIAGEN) (*79*). Total RNA concentration was measured using a NanoDrop 2000 spectrophotometer (Thermo Fisher Scientific). mRNA reverse transcription was performed to synthesize cDNA by using High Capacity cDNA Reverse Transcription Kit (Applied Biosystems, catalog no. 4368814). Target gene expressions were determined by quantitative reverse transcription PCR by using specific TaqMan Gene Expression assays or SYBR Green assays. Target gene expression levels were normalized to *Gapdh* mRNA levels. The experiments were performed in triplicate with three lines per group, and the ΔCT method was used to calculate the target gene expression levels. The sequences of the SYBR Green primers used are listed in table S3.

Chromatin immunoprecipitation

We performed ChIP by using cross-linked lysate from FLNC homozygous KO iPSC-CMs and control iPSC-CMs according to the manufacturer's instructions (ChIP-IT High Sensitivity; ACTIVE MOTIF; catalog no. 53040). iPSC-CMs were fixed with formaldehyde to cross-link the protein/DNA complexes. DNA was then sheared into small fragments by sonication; the sheared DNA was then incubated with anti–β-catenin (ChIP grade) and precipitated using Protein G agarose beads to pull down the complexes of interest. Next, the pull-down cross-linked products were reversed and digested with Proteinase K, and the DNA was recovered and purified for qPCR. The primers for *SOX2* binding region were 5′-TTCAGACCACCCAGTCTTGT-3′ and 5′-CCGTTTTGAACTAGGGGTCT-3′; primers for *SOX9* binding region were 5′-AGGCCTTTAAACCTTCCAGA-3′ and 5′-AAAGCAGAAAGCAATGGATG-3′; NFKB primers were 5′-ATCAGAGAGCGATGAAGGTG-3′ and 5′-GATGCTCCAGGAACCAGAC-3′.

RNA sequencing

RNA-seq was performed on RNA depleted of ribosomal RNA (rRNA) extracted from the iPSC-CMs on an Illumina platform, as previously published (*79*). Briefly, total RNA was extracted from the whole heart and the concentration of each RNA sample was determined using a NanoDrop Spectrophotometer. RNA samples were then electrophoretic separated on an Agilent Bioanalyzer RNA chip for RNA integrity test and samples with an RNA integrity number >8 were used to prepare sequencing library using the Illumina TruSeq stranded total RNA library preparation kit. Before RNA library construction, RNA samples were depleted of rRNA using the EpiCentre Ribo-Zero Gold Magnetic Kit. The RNA samples were sequenced on the Illumina HiSeq 4000 instrument using the paired-end sample preparation chemistry.

RNA-seq data analysis

For each sample, about 20 million to 30 million pairs of 150–base pair paired-end reads were generated. Raw reads were first trimmed for 10 bases at the 5′ end to remove reads with biased nucleotide (ACGT) distribution. Trimmed reads were then aligned to the *Mus musculus* genome (GRCh38, GENCODE, version 28 and 34, primary assembly) using STAR aligner (*80*) (version 2.5.0a). DEG analyses on the read counts were performed using DESeq2 (*81*) (v1.22.2) in R environment. Genes with mean read counts less than 10 across samples were filtered out from analysis. A gene was considered significantly dysregulated if the adjusted *P* values are less than 10% and there is a twofold change based on shrunken $\log_2$ fold change implemented in DESeq2 [false discovery rate < 0.01 and abs($\log_2$FC) > 1]. Expression heatmaps were generated using pheatmap package in R environment. Functional enrichment of the significantly dysregulated genes was carried out using DAVID (*82*) and GSEA software (*83*).

Statistics

Statistical analyses were performed as previously described (*84*). Experimental outcomes were expressed as means ± SD. Statistically

Downloaded from https://www.science.org at Universita degli Studi di Trieste on March 30, 2022

significant differences were determined by *t* test between two groups and one-way analysis of variance (ANOVA) among multiple groups, followed by pairwise comparison. Experimental data that did not follow normal distribution were analyzed by the Kruskal-Wallis test. All statistical analyses were performed using GraphPad Prism 8.

SUPPLEMENTARY MATERIALS

Supplementary material for this article is available at https://science.org/doi/10.1126/sciadv.abk0052

View/request a protocol for this paper from *Bio–protocol*.

REFERENCES AND NOTES

1. R. E. Hershberger, J. D. Siegfried, Update 2011: Clinical and genetic issues in familial dilated cardiomyopathy. *J. Am. Coll. Cardiol.* **57**, 1641–1649 (2011).
2. D. Nandi, J. W. Rossano, Epidemiology and cost of heart failure in children. *Cardiol. Young* **25**, 1460–1468 (2015).
3. J. A. Towbin, A. Lorts, Arrhythmias and dilated cardiomyopathy. *J. Am. Coll. Cardiol.* **57**, 2169–2171 (2011).
4. W. J. McKenna, B. J. Maron, G. Thiene, Classification, epidemiology, and global burden of cardiomyopathies. *Circ. Res.* **121**, 722–730 (2017).
5. R. E. Hershberger, D. J. Hedges, A. Morales, Dilated cardiomyopathy: The complexity of a diverse genetic architecture. *Nat. Rev. Cardiol.* **10**, 531–547 (2013).
6. R. L. Begay, S. L. Graw, G. Sinagra, A. Asimaki, T. J. Rowland, D. B. Slavov, K. Gowan, K. L. Jones, F. Brun, M. Merlo, D. Miani, M. Sweet, K. Devaraj, E. P. Wartchow, M. Gigli, I. Puggia, E. E. Salcedo, D. M. Garrity, A. V. Ambardekar, P. Buttrick, T. B. Reece, M. R. Bristow, J. E. Saffitz, L. Mestroni, M. R. G. Taylor, Filamin C truncation mutations are associated with arrhythmogenic dilated cardiomyopathy and changes in the cell–cell adhesion structures. *JACC Clin. Electrophysiol.* **4**, 504–514 (2018).
7. R. L. Begay, C. A. Tharp, A. Martin, S. L. Graw, G. Sinagra, D. Miani, M. E. Sweet, D. B. Slavov, N. Stafford, M. J. Zeller, R. Alnefaie, T. J. Rowland, F. Brun, K. L. Jones, K. Gowan, L. Mestroni, D. M. Garrity, M. R. G. Taylor, FLNC gene splice mutations cause dilated cardiomyopathy. *JACC Basic Transl. Sci.* **1**, 344–359 (2016).
8. A. X. Zhou, J. H. Hartwig, L. M. Akyurek, Filamins in cell signaling, transcription and organ development. *Trends Cell Biol.* **20**, 113–123 (2010).
9. Z. Razinia, T. Makela, J. Ylanne, D. A. Calderwood, Filamins in mechanosensing and signaling. *Annu. Rev. Biophys.* **41**, 227–246 (2012).
10. A. Brodehl, R. A. Ferrier, S. J. Hamilton, S. C. Greenway, M. A. Brundler, W. Yu, W. T. Gibson, M. L. McKinnon, B. McGillivray, N. Alvarez, M. Giuffre, J. Schwartzentruber; FORGE Canada Consortium, B. Gerull, Mutations in *FLNC* are associated with familial restrictive cardiomyopathy. *Hum. Mutat.* **37**, 269–279 (2016).
11. R. Valdes-Mas, A. Gutiérrez-Fernández, J. Gómez, E. Coto, A. Astudillo, D. A. Puente, J. R. Reguero, V. Álvarez, C. Morís, D. León, M. Martín, X. S. Puente, C. López-Otín, Mutations in filamin C cause a new form of familial hypertrophic cardiomyopathy. *Nat. Commun.* **5**, 5326 (2014).
12. N. R. Tucker, M. A. McLellan, D. Hu, J. Ye, V. A. Parsons, R. W. Mills, S. Clauss, E. Dolmatova, M. A. Shea, D. J. Milan, N. S. Scott, M. Lindsay, S. A. Lubitz, I. J. Domian, J. R. Stone, H. Lin, P. T. Ellinor, Novel mutation in *FLNC* (Filamin C) causes familial restrictive cardiomyopathy. *Circ. Cardiovasc. Genet.* **10**, (2017).
13. J. Bloomekatz, R. Singh, O. W. J. Prall, A. C. Dunn, M. Vaughan, C. S. Loo, R. P. Harvey, D. Yelon, Platelet-derived growth factor (PDGF) signaling directs cardiomyocyte movement toward the midline during heart tube assembly. *eLife* **6**, (2017).
14. M. D. Tallquist, W. J. French, P. Soriano, Additive effects of PDGF receptor beta signaling pathways in vascular smooth muscle cell development. *PLOS Biol.* **1**, E52 (2003).
15. M. D. Tallquist, P. Soriano, Cell autonomous requirement for PDGFRalpha in populations of cranial and cardiac neural crest cells. *Development* **130**, 507–518 (2003).
16. R. Lombardi, S. N. Chen, A. Ruggiero, P. Gurha, G. Z. Czernuszewicz, J. T. Willerson, A. J. Marian, Cardiac fibro-adipocyte progenitors express desmosome proteins and preferentially differentiate to adipocytes upon deletion of the desmoplakin gene. *Circ. Res.* **119**, 41–54 (2016).
17. A. Eriksson, A. Siegbahn, B. Westermark, C. H. Heldin, L. Claesson-Welsh, PDGF alpha- and beta-receptors activate unique and common signal transduction pathways. *EMBO J.* **11**, 543–550 (1992).
18. C. E. Hart, J. W. Forstrom, J. D. Kelly, R. A. Seifert, R. A. Smith, R. Ross, M. J. Murray, D. F. Bowen-Pope, Two classes of PDGF receptor recognize different isoforms of PDGF. *Science* **240**, 1529–1531 (1988).
19. C. Constantinou, A. M. A. Miranda, P. Chaves, M. Bellahcene, A. Massaia, K. Cheng, S. Samari, S. M. Rothery, A. M. Chandler, R. P. Schwarz, S. E. Harding, P. Punjabi, M. D. Schneider, M. Noseda, Human pluripotent stem cell-derived cardiomyocytes as a target platform for paracrine protection by cardiac mesenchymal stromal cells. *Sci. Rep.* **10**, 13016 (2020).
20. M. P. Santini, E. Forte, R. P. Harvey, J. C. Kovacic, Developmental origin and lineage plasticity of endogenous cardiac stem cells. *Development* **143**, 1242–1258 (2016).
21. M. Noseda, M. Harada, S. McSweeney, T. Leja, E. Belian, D. J. Stuckey, M. S. Abreu Paiva, J. Habib, I. Macaulay, A. J. de Smith, F. al-Beidh, R. Sampson, R. T. Lumbers, P. Rao, S. E. Harding, A. I. F. Blakemore, S. Eirik Jacobsen, M. Barahona, M. D. Schneider, PDGFRα demarcates the cardiogenic clonogenic Sca1+ stem/progenitor cell in adult murine myocardium. *Nat. Commun.* **6**, 6930 (2015).
22. S. El-Rass, S. Eisa-Beygi, E. Khong, K. Brand-Arzamendi, A. Mauro, H. Zhang, K. J. Clark, S. C. Ekker, X.-Y. Wen, Disruption of *pdgfra* alters endocardial and myocardial fusion during zebrafish cardiac assembly. *Biol Open* **6**, 348–357 (2017).
23. J. Lee, V. Termglinchan, S. Diecke, I. Itzhaki, C. K. Lam, P. Garg, E. Lau, M. Greenhaw, T. Seeger, H. Wu, J. Z. Zhang, X. Chen, I. P. Gil, M. Ameen, K. Sallam, J. W. Rhee, J. M. Churko, R. Chaudhary, T. Chour, P. J. Wang, M. P. Snyder, H. Y. Chang, I. Karakikes, J. C. Wu, Activation of PDGF pathway links LMNA mutation to dilated cardiomyopathy. *Nature* **572**, 335–340 (2019).
24. M. Valius, A. Kazlauskas, Phospholipase C-gamma 1 and phosphatidylinositol 3 kinase are the downstream mediators of the PDGF receptor's mitogenic signal. *Cell* **73**, 321–334 (1993).
25. D. Matei, R. E. Emerson, Y. C. Lai, L. A. Baldridge, J. Rao, C. Yiannoutsos, D. D. Donner, Autocrine activation of PDGFRalpha promotes the progression of ovarian cancer. *Oncogene* **25**, 2060–2069 (2006).
26. F. Brun, M. Gigli, S. L. Graw, D. P. Judge, M. Merlo, B. Murray, H. Calkins, G. Sinagra, M. R. G. Taylor, L. Mestroni, C. A. James, *FLNC* truncations cause arrhythmogenic right ventricular cardiomyopathy. *J. Med. Genet.* **57**, 254–257 (2020).
27. S. Diecke, J. Lu, J. Lee, V. Termglinchan, N. G. Kooreman, P. W. Burridge, A. D. Ebert, J. M. Churko, A. Sharma, M. A. Kay, J. C. Wu, Novel codon-optimized mini-intronic plasmid for efficient, inexpensive, and xeno-free induction of pluripotency. *Sci. Rep.* **5**, 8081 (2015).
28. P. W. Burridge, E. Matsa, P. Shukla, Z. C. Lin, J. M. Churko, A. D. Ebert, F. Lan, S. Diecke, B. Huber, N. M. Mordwinkin, J. R. Plews, O. J. Abilez, B. Cui, J. D. Gold, J. C. Wu, Chemically defined generation of human cardiomyocytes. *Nat. Methods* **11**, 855–860 (2014).
29. E. D. Cohen, K. Ihida-Stansbury, M. M. Lu, R. A. Panettieri, P. L. Jones, E. E. Morrisey, Wnt signaling regulates smooth muscle precursor development in the mouse lung via a tenascin C/PDGFR pathway. *J. Clin. Invest.* **119**, 2538–2549 (2009).
30. T. L. Kuo, K. H. Cheng, Y. S. Shan, L. T. Chen, W. C. Hung, β-catenin-activated autocrine PDGF/Src signaling is a therapeutic target in pancreatic cancer. *Theranostics* **9**, 324–336 (2019).
31. J. Takahashi, M. Orcholski, K. Yuan, V. de Jesus Perez, PDGF-dependent β-catenin activation is associated with abnormal pulmonary artery smooth muscle cell proliferation in pulmonary arterial hypertension. *FEBS Lett.* **590**, 101–109 (2016).
32. M. Z. Hossain, P. Ao, A. L. Boynton, Rapid disruption of gap junctional communication and phosphorylation of connexin43 by platelet-derived growth factor in T51B rat liver epithelial cells expressing platelet-derived growth factor receptor. *J. Cell. Physiol.* **174**, 66–77 (1998).
33. M. Z. Hossain, P. Ao, A. L. Boynton, Platelet-derived growth factor-induced disruption of gap junctional communication and phosphorylation of connexin43 involves protein kinase C and mitogen-activated protein kinase. *J. Cell. Physiol.* **176**, 332–341 (1998).
34. M. Z. Hossain, A. B. Jagdale, P. Ao, A. Kazlauskas, A. L. Boynton, Disruption of gap junctional communication by the platelet-derived growth factor is mediated via multiple signaling pathways. *J. Biol. Chem.* **274**, 10489–10496 (1999).
35. S. Kurtenbach, S. Kurtenbach, G. Zoidl, Gap junction modulation and its implications for heart function. *Front. Physiol.* **5**, 82 (2014).
36. E. Leithe, E. Rivedal, Epidermal growth factor regulates ubiquitination, internalization and proteasome-dependent degradation of connexin43. *J. Cell Sci.* **117**, 1211–1220 (2004).
37. K. Leykauf, M. Durst, A. Alonso, Phosphorylation and subcellular distribution of connexin43 in normal and stressed cells. *Cell Tissue Res.* **311**, 23–30 (2003).
38. R. J. Ruch, J. E. Trosko, B. V. Madhukar, Inhibition of connexin43 gap junctional intercellular communication by TPA requires ERK activation. *J. Cell. Biochem.* **83**, 163–169 (2001).
39. S. B. Danik, F. Liu, J. Zhang, H. J. Suk, G. E. Morley, G. I. Fishman, D. E. Gutstein, Modulation of cardiac gap junction expression and arrhythmic susceptibility. *Circ. Res.* **95**, 1035–1041 (2004).
40. D. E. Gutstein, G. E. Morley, D. Vaidya, F. Liu, F. L. Chen, H. Stuhlmann, G. I. Fishman, Heterogeneous expression of Gap junction channels in the heart leads to conduction defects and ventricular dysfunction. *Circulation* **104**, 1194–1199 (2001).
41. S. Poelzing, D. S. Rosenbaum, Altered connexin43 expression produces arrhythmia substrate in heart failure. *Am. J. Physiol. Heart Circ. Physiol.* **287**, H1762–H1770 (2004).
42. D. O. Furst, L. G. Goldfarb, R. A. Kley, M. Vorgerd, M. Olivé, P. F. M. van der Ven, Filamin C-related myopathies: Pathology and mechanisms. *Acta Neuropathol.* **125**, 33–46 (2013).
43. P. F. van der Ven, W. M. Obermann, B. Lemke, M. Gautel, K. Weber, D. O. Fürst, Characterization of muscle filamin isoforms suggests a possible role of gamma-filamin/ABP-L in sarcomeric Z-disc formation. *Cell Motil. Cytoskeleton* **45**, 149–162 (2000).

Downloaded from https://www.science.org at Universita degli Studi di Trieste on March 30, 2022

44. B. Gerull, A. Heuser, T. Wichter, M. Paul, C. T. Basson, D. McDermott, B. B. Lerman, S. M. Markowitz, P. T. Ellinor, C. MacRae, S. Peters, K. S. Grossmann, J. Drenckhahn, B. Michely, S. Sasse-Klaassen, W. Birchmeier, R. Dietz, G. Breithardt, E. Schulze-Bahr, L. Thierfelder, Mutations in the desmosomal protein plakophilin-2 are common in arrhythmogenic right ventricular cardiomyopathy. *Nat. Genet.* **36**, 1162–1164 (2004).
45. A. Rampazzo, A. Nava, S. Malacrida, G. Beffagna, B. Bauce, V. Rossi, R. Zimbello, B. Simionati, C. Basso, G. Thiene, J. A. Towbin, G. A. Danieli, Mutation in human desmoplakin domain binding to plakoglobin causes a dominant form of arrhythmogenic right ventricular cardiomyopathy. *Am. J. Hum. Genet.* **71**, 1200–1206 (2002).
46. K. Pilichou, A. Nava, C. Basso, G. Beffagna, B. Bauce, A. Lorenzon, G. Frigo, A. Vettori, M. Valente, J. Towbin, G. Thiene, G. A. Danieli, A. Rampazzo, Mutations in desmoglein-2 gene are associated with arrhythmogenic right ventricular cardiomyopathy. *Circulation* **113**, 1171–1179 (2006).
47. P. Syrris, D. Ward, A. Evans, A. Asimaki, E. Gandjbakhch, S. Sen-Chowdhry, W. J. McKenna, Arrhythmogenic right ventricular dysplasia/cardiomyopathy associated with mutations in the desmosomal gene desmocollin-2. *Am. J. Hum. Genet.* **79**, 978–984 (2006).
48. S. Gao, D. Puthenvedu, R. Lombardi, S. N. Chen, Established and emerging mechanisms in the pathogenesis of arrhythmogenic cardiomyopathy: A multifaceted disease. *Int. J. Mol. Sci.* **21**, (2020).
49. Z. Mao, F. Nakamura, Structure and function of filamin C in the muscle Z-Disc. *Int. J. Mol. Sci.* **21**, (2020).
50. Y. Zhou, Z.'. Chen, L. Zhang, M. Zhu, C. Tan, X. Zhou, S. M. Evans, X. Fang, W. Feng, J. Chen, Loss of filamin C Is catastrophic for heart function. *Circulation* **141**, 869–871 (2020).
51. J. Li, D. Swope, N. Raess, L. Cheng, E. J. Muller, G. L. Radice, Cardiac tissue-restricted deletion of plakoglobin results in progressive cardiomyopathy and activation of {beta}-catenin signaling. *Mol. Cell. Biol.* **31**, 1134–1144 (2011).
52. C. S. Cselenyi, K. K. Jernigan, E. Tahinci, C. A. Thorne, L. A. Lee, E. Lee, LRP6 transduces a canonical Wnt signal independently of Axin degradation by inhibiting GSK3's phosphorylation of beta-catenin. *Proc. Natl. Acad. Sci. U.S.A.* **105**, 8032–8037 (2008).
53. K. Mi, P. J. Dolan, G. V. Johnson, The low density lipoprotein receptor-related protein 6 interacts with glycogen synthase kinase 3 and attenuates activity. *J. Biol. Chem.* **281**, 4787–4794 (2006).
54. S. Piao, S. H. Lee, H. Kim, S. Yum, J. L. Stamos, Y. Xu, S. J. Lee, J. Lee, S. Oh, J. K. Han, B. J. Park, W. I. Weis, N. C. Ha, Direct inhibition of GSK3beta by the phosphorylated cytoplasmic domain of LRP6 in Wnt/beta-catenin signaling. *PLOS ONE* **3**, e4046 (2008).
55. F. Fagotto, N. Funayama, U. Gluck, B. M. Gumbiner, Binding to cadherins antagonizes the signaling activity of beta-catenin during axis formation in Xenopus. *J. Cell Biol.* **132**, 1105–1114 (1996).
56. J. Heasman, A. Crawford, K. Goldstone, P. Garner-Hamrick, B. Gumbiner, P. McCrea, C. Kintner, C. Y. Noro, C. Wylie, Overexpression of cadherins and underexpression of beta-catenin inhibit dorsal mesoderm induction in early Xenopus embryos. *Cell* **79**, 791–803 (1994).
57. S. Orsulic, O. Huber, H. Aberle, S. Arnold, R. Kemler, E-cadherin binding prevents beta-catenin nuclear localization and beta-catenin/LEF-1-mediated transactivation. *J. Cell Sci.* **112**(Pt 8), 1237–1245 (1999).
58. O. Huber, R. Korn, J. McLaughlin, M. Ohsugi, B. G. Herrmann, R. Kemler, Nuclear localization of beta-catenin by interaction with transcription factor LEF-1. *Mech. Dev.* **59**, 3–10 (1996).
59. M. H. Wong, B. Rubinfeld, J. I. Gordon, Effects of forced expression of an NH2-terminal truncated beta-Catenin on mouse intestinal epithelial homeostasis. *J. Cell Biol.* **141**, 765–777 (1998).
60. M. C. Ferreira-Cornwell, Y. Luo, N. Narula, J. M. Lenox, M. Lieberman, G. L. Radice, Remodeling the intercalated disc leads to cardiomyopathy in mice misexpressing cadherins in the heart. *J. Cell Sci.* **115**, 1623–1634 (2002).
61. I. Kostetskii, J. Li, Y. Xiong, R. Zhou, V. A. Ferrari, V. V. Patel, J. D. Molkentin, G. L. Radice, Induced deletion of the N-cadherin gene in the heart leads to dissolution of the intercalated disc structure. *Circ. Res.* **96**, 346–354 (2005).
62. V. Chintalgattu, D. Ai, R. R. Langley, J. Zhang, J. A. Bankson, T. L. Shih, A. K. Reddy, K. R. Coombes, I. N. Daher, S. Pati, S. S. Patel, J. S. Pocius, G. E. Taffet, L. M. Buja, M. L. Entman, A. Y. Khakoo, Cardiomyocyte PDGFR-beta signaling is an essential component of the mouse cardiac response to load-induced stress. *J. Clin. Invest.* **120**, 472–484 (2010).
63. J. J. Chong, H. Reinecke, M. Iwata, B. Torok-Storb, A. Stempien-Otero, C. E. Murry, Progenitor cells identified by PDGFR-alpha expression in the developing and diseased human heart. *Stem Cells Dev.* **22**, 1932–1943 (2013).
64. J. Waaler, O. Machon, J. P. von Kries, S. R. Wilson, E. Lundenes, D. Wedlich, D. Gradl, J. E. Paulsen, O. Machonova, J. L. Dembinski, H. Dinh, S. Krauss, Novel synthetic antagonists of canonical Wnt signaling inhibit colorectal cancer cell growth. *Cancer Res.* **71**, 197–205 (2011).
65. D. Fang, D. Hawke, Y. Zheng, Y. Xia, J. Meisenhelder, H. Nika, G. B. Mills, R. Kobayashi, T. Hunter, Z. Lu, Phosphorylation of beta-catenin by AKT promotes beta-catenin transcriptional activity. *J. Biol. Chem.* **282**, 11221–11229 (2007).
66. L. Han, Y. Yang, X. Yue, K. Huang, X. Liu, P. Pu, H. Jiang, W. Yan, T. Jiang, C. Kang, Inactivation of PI3K/AKT signaling inhibits glioma cell growth through modulation of β-catenin-mediated transcription. *Brain Res.* **1366**, 9–17 (2010).
67. J. L. Solan, P. D. Lampe, Connexin43 phosphorylation: Structural changes and biological effects. *Biochem. J.* **419**, 261–272 (2009).
68. G. S. Orphanos, G. N. Ioannidis, A. G. Ardavanis, Cardiotoxicity induced by tyrosine kinase inhibitors. *Acta Oncol.* **48**, 964–970 (2009).
69. A. Sharma, P. W. Burridge, W. L. McKeithan, R. Serrano, P. Shukla, N. Sayed, J. M. Churko, T. Kitani, H. Wu, A. Holmström, E. Matsa, Y. Zhang, A. Kumar, A. C. Fan, J. C. del Álamo, S. M. Wu, J. J. Moslehi, M. Mercola, J. C. Wu, High-throughput screening of tyrosine kinase inhibitor cardiotoxicity with human induced pluripotent stem cells. *Sci. Transl. Med.* **9**, (2017).
70. H. Wang, R. P. Sheehan, A. C. Palmer, R. A. Everley, S. A. Boswell, N. Ron-Harel, A. E. Ringel, K. M. Holton, C. A. Jacobson, A. R. Erickson, L. Maliszewski, M. C. Haigis, P. K. Sorger, Adaptation of human iPSC-derived cardiomyocytes to tyrosine kinase inhibitors reduces acute cardiotoxicity via metabolic reprogramming. *Cell Syst.* **8**, 412–426.e7 (2019).
71. C. K. Lam, J. C. Wu, Clinical trial in a dish. *Arterioscler. Thromb. Vasc. Biol.* **41**, 1019–1031 (2021).
72. C. C. Smith, E. A. Lasater, K. C. Lin, Q. Wang, M. Q. McCreery, W. K. Stewart, L. E. Damon, A. E. Perl, G. R. Jeschke, M. Sugita, M. Carroll, S. C. Kogan, J. Kuriyan, N. P. Shah, Crenolanib is a selective type I pan-FLT3 inhibitor. *Proc. Natl. Acad. Sci. U.S.A.* **111**, 5319–5324 (2014).
73. L. Mestroni, B. Maisch, W. J. McKenna, K. Schwartz, P. Charron, C. Rocco, F. Tesson, A. Richter, A. Wilke, M. Komajda, Guidelines for the study of familial dilated cardiomyopathies. Collaborative Research Group of the European Human and Capital Mobility Project on Familial Dilated Cardiomyopathy. *Eur. Heart J.* **20**, 93–102 (1999).
74. M. Gigli, M. Merlo, S. L. Graw, G. Barbati, T. J. Rowland, D. B. Slavov, D. Stolfo, M. E. Haywood, M. D. Ferro, A. Altinier, F. Ramani, F. Brun, A. Cocciolo, I. Puggia, G. Morea, W. J. Mc Kenna, F. G. La Rosa, M. R. G. Taylor, G. Sinagra, L. Mestroni, Genetic risk of arrhythmic phenotypes in patients with dilated cardiomyopathy. *J. Am. Coll. Cardiol.* **74**, 1480–1490 (2019).
75. F. I. Marcus, W. J. McKenna, D. Sherrill, C. Basso, B. Bauce, D. A. Bluemke, H. Calkins, D. Corrado, M. G. P. J. Cox, J. P. Daubert, G. Fontaine, K. Gear, R. Hauer, A. Nava, M. H. Picard, N. Protonotarios, J. E. Saffitz, D. M. Yoerger Sanborn, J. S. Steinberg, H. Tandri, G. Thiene, J. A. Towbin, A. Tsatsopoulou, T. Wichter, W. Zareba, Diagnosis of arrhythmogenic right ventricular cardiomyopathy/dysplasia: Proposed modification of the task force criteria. *Circulation* **121**, 1533–1541 (2010).
76. M. E. Haywood, M. E. Haywood, A. Cocciolo, K. F. Porter, E. Dobrinskikh, D. Slavov, S. L. Graw, T. Brett Reece, A. V. Ambardekar, M. R. Bristow, L. Mestroni, M. R. G. Taylor, Transcriptome signature of ventricular arrhythmia in dilated cardiomyopathy reveals increased fibrosis and activated TP53. *J. Mol. Cell. Cardiol.* **139**, 124–134 (2020).
77. C. K. Lam, L. Tian, N. Belbachir, A. Wnorowski, R. Shrestha, N. Ma, T. Kitani, J.-W. Rhee, J. C. Wu, Identifying the transcriptome signatures of calcium channel blockers in human induced pluripotent stem cell-derived cardiomyocytes. *Circ. Res.* **125**, 212–222 (2019).
78. J. Z. Zhang, V. Termglinchan, N.-Y. Shao, I. Itzhaki, C. Liu, N. Ma, L. Tian, V. Y. Wang, A. C. Y. Chang, H. Guo, T. Kitani, H. Wu, C. K. Lam, K. Kodo, N. Sayed, H. M. Blau, J. C. Wu, A human iPSC double-reporter system enables purification of cardiac lineage subpopulations with distinct function and drug response profiles. *Cell Stem Cell* **24**, 802–811.e5 (2019).
79. S. N. Chen, P. Gurha, R. Lombardi, A. Ruggiero, J. T. Willerson, A. J. Marian, The hippo pathway is activated and is a causal mechanism for adipogenesis in arrhythmogenic cardiomyopathy. *Circ. Res.* **114**, 454–468 (2014).
80. K. Vezendi, F. Krizsa, I. Szabo, I. Cserhati, The effect of platelet homogenate fractions on megakaryocytopoiesis in the mouse. *Haematologia* **19**, 113–116 (1986).
81. M. I. Love, W. Huber, S. Anders, Moderated estimation of fold change and dispersion for RNA-seq data with DESeq2. *Genome Biol.* **15**, 550 (2014).
82. D. W. Huang, B. T. Sherman, R. A. Lempicki, Systematic and integrative analysis of large gene lists using DAVID bioinformatics resources. *Nat. Protoc.* **4**, 44–57 (2009).
83. A. Subramanian, P. Tamayo, V. K. Mootha, S. Mukherjee, B. L. Ebert, M. A. Gillette, A. Paulovich, S. L. Pomeroy, T. R. Golub, E. S. Lander, J. P. Mesirov, Gene set enrichment analysis: A knowledge-based approach for interpreting genome-wide expression profiles. *Proc. Natl. Acad. Sci. U.S.A.* **102**, 15545–15550 (2005).
84. R. Lombardi, J. Dong, G. Rodriguez, A. Bell, T. K. Leung, R. J. Schwartz, J. T. Willerson, R. Brugada, A. J. Marian, Genetic fate mapping identifies second heart field progenitor cells as a source of adipocytes in arrhythmogenic right ventricular cardiomyopathy. *Circ. Res.* **104**, 1076–1084 (2009).

Acknowledgments: We would like to acknowledge D. Slavov for his technical contribution in generating the FLNC knockout iPSCs using the CRISPR-Cas technology. **Funding:** This work was supported by Career Development Award from the American Heart Association 19CDA34660035 to S.N.C. and 19CDA34770040 to C.K.L. and the Boettcher Foundation to S.N.C. In addition, this work was supported by NIH R01HL69071, R01HL116906, R01HL147064,

Downloaded from https://www.science.org at Universita degli Studi di Trieste on March 30, 2022

and AHA 17GRNT33670495 to L.M.; NIH 1K23HI067915 and R01HL109209 to M.R.G.T.; Trans-Atlantic Network of Excellence grant from the Fondation Leducq (14-CVD03) to L.M. and M.R.G.T.; and NIH R01 HL113006, R01 HL126527, R01 HL123968, R01 HL141851, R01 HL130020, and P01 HL141084 to J.C.W. This work was also supported by NIH/NCATS Colorado CTSA Grant Number UL1 TR001082 (contents are the authors' sole responsibility and do not necessarily represent official NIH views). **Author contributions:** S.N.C. and C.K.L. wrote the original draft. S.N.C. and C.K.L. designed, conceptualized, and supervised experiments. S.N.C., C.K.L., S.Ga., O.A.M., and S.R.Z. performed experiments. Y.-W.W. performed bioinformatics analysis. L.M., M.R.G.T., G.S., A.V.A., M.R.B., and J.C. contributed to patient recruitment and clinical findings. S.N.C., C.K.L., M.R.B., M.R.G.T., L.M. and J.C.W. were responsible for funding acquisition. S.N.C., C.K.L., R.L., J.C.W., M.R.G.T., and L.M. contributed to the conceptual content and editing of the manuscript. All authors reviewed the manuscript. **Competing interests:** J.C.W. is a cofounder of Greenstone Biosciences but has no competing interests, as the work presented here is completely independent. All other authors declare that they have no competing interests. **Data and materials availability**: All data needed to evaluate the conclusions in the paper are present in the paper and/or the Supplementary Materials. The human iPSC models in this study can be provided by J.C.W., L.M., and S.N.C. pending scientific review and a completed material transfer agreement. Requests for the iPSC models should be submitted to S.N.C.: suet.chen@cuanschutz.edu.

Submitted 15 June 2021
Accepted 25 December 2021
Published 23 February 2022
10.1126/sciadv.abk0052

Downloaded from https://www.science.org at Universita degli Studi di Trieste on March 30, 2022

ScienceAdvances

Activation of PDGFRA signaling contributes to filamin C–related arrhythmogenic cardiomyopathy

Suet Nee ChenChi Keung LamYing-Wooi WanShanshan GaoOlfat A. MalakShane Rui ZhaoRaffaella LombardiAmrut V. AmbardekarMichael R. BristowJoseph ClevelandMarta GigliGianfranco SinagraSharon GrawMatthew R.G. TaylorJoseph C. WuLuisa Mestroni

Sci. Adv., 8 (8), eabk0052. • DOI: 10.1126/sciadv.abk0052

View the article online
https://www.science.org/doi/10.1126/sciadv.abk0052
Permissions
https://www.science.org/help/reprints-and-permissions

Downloaded from https://www.science.org at Universita degli Studi di Trieste on March 30, 2022

Use of this article is subject to the Terms of service

Science Advances (ISSN) is published by the American Association for the Advancement of Science. 1200 New York Avenue NW, Washington, DC 20005. The title *Science Advances* is a registered trademark of AAAS.
Copyright © 2022 The Authors, some rights reserved; exclusive licensee American Association for the Advancement of Science. No claim to original U.S. Government Works. Distributed under a Creative Commons Attribution NonCommercial License 4.0 (CC BY-NC).